

The effects of polarization on the observables in the decay $\Xi_{cc}^{++} \rightarrow \Xi_c^+ \bar{\ell} \nu_\ell$

Qazi Maaz Us Salam,^{a,b} Anamta Asif,^{1a} Ishtiaq Ahmed,^b Rizwan Khalid^a

^a*School of Science and Engineering, Lahore University of Management Sciences (LUMS), Opposite Sector U, D.H.A, Lahore 54792, Pakistan*

^b*National Center for Physics, Shahdra Valley Road, Islamabad 44000, Pakistan*

E-mail: qazimaaz92@gmail.com, 25100098@lums.edu.pk,
ishtiaq.ahmed@ncp.edu.pk, rizwan_khalid@lums.edu.pk

ABSTRACT: We investigate the effects of polarization on several physical observables in the semileptonic decay $\Xi_{cc}^{++} \rightarrow \Xi_c^+ \bar{\ell} \nu_\ell$. We analyze the polarization effects of the particles involved in the decay, namely Ξ_{cc}^{++} , Ξ_c^+ , and the charged muon ℓ . Using the form factors obtained from QCD sum rules, we compute the q^2 -dependent observables including the differential branching ratio, forward–backward asymmetry, and polarization asymmetries for both longitudinal and transverse polarization states. We also define and examine several polarization ratios and discuss correlations among different observables. In addition, we evaluate the lepton flavor universality ratio defined as $\mathcal{R}_{\Xi_c^+}(\mu/e) \equiv \mathcal{D}(\Xi_{cc}^{++} \rightarrow \Xi_c^+ \mu^+ \nu_\mu) / \mathcal{D}(\Xi_{cc}^{++} \rightarrow \Xi_c^+ e^+ \nu_e)$ and analyze its behavior over the available dynamical range. Our results show that these observables are quite sensitive to polarization effects a study of which provides excellent probes for testing the Standard Model.

¹Corresponding author

Contents

1	Introduction	2
2	Theoretical Framework	4
3	Phenomenological study	7
3.1	Input parameters	7
3.2	Observables focusing on one particle at a time	7
3.2.1	Polarized (m, n) cases	8
3.3	Lepton-Flavor Universality	14
3.4	Polarization Asymmetry Analysis	14
3.4.1	Polarization Asymmetry $P^{(m,n)}$	15
3.4.2	Polarization Ratios $\mathcal{R}_{nn'}^{(m,m')}[j]$	16
3.4.3	Polarization Asymmetry Ratios $\mathcal{R}_{P_{nn'}^{(m,m')}}^{(m,m')}$	17
3.5	Correlation Analysis of Polarized Observables	19
4	Summary and Conclusion	20
A	Tables of Numerical Results	21
B	Decay Amplitudes for Polarized Particles	23

1 Introduction

The semileptonic decays of heavy baryons offer valuable insight into the dynamics of heavy flavor and weak interactions. Among these processes, the study of flavor changing charged current (FCCC) interactions which occur at the quark level through decay of a heavy quark to a light one in conjunction with a lepton-antineutrino/antilepton-neutrino pair is interesting. Such studies provide information about the Cabibbo-Kobayashi-Maskawa (CKM) matrix elements, as well as the structure of the weak effective Hamiltonian. In this manuscript, we analyze in detail the decay $\Xi_{cc}^{++} \rightarrow \Xi_c^+ \ell^+ \nu_\ell$, which at the quark level corresponds to the transition $c \rightarrow s$, making it sensitive to the CKM matrix element $|V_{cs}|$. This decay also serves as a testing ground for heavy quark effective theory (HQET) symmetries in the baryon sector.

The quark model [1] has been crucial in describing various features of hadron spectroscopy. Whereas many particles theorized by the model still need to be confirmed experimentally, a large number of doubly heavy baryons have been identified. One such baryon is $\Xi_{cc}^+(3520)$, which was first observed by the SELEX collaboration in 2002 via its decay to pD^+K^- [2]. Similarly, the doubly charmed baryon $\Xi_{cc}^{++}(3621)$ was confirmed in the

LHCb experiment in 2017, making use of the $\Xi_{cc}^{++} \rightarrow \Lambda_c^+ K^- \pi^+ \pi^+$ channel [3]. Subsequent experiments had been carried out in search for the Ξ_{cc}^+ through the decay channels $\Xi_{cc}^+ \rightarrow \Lambda_c^+ K^- \pi^+$ in 2019 [4] and $\Xi_{cc}^+ \rightarrow \Xi_c^+ \pi^+ \pi^-$ in 2021 by the LHCb collaboration [5]. The combined result of these three experiments concluded with a local significance of 4.0 standard deviations for the mass of Ξ_{cc}^+ [5] to be 3620 MeV, showing a minimal gap between the masses of Ξ_{cc}^+ and Ξ_{cc}^{++} . The search for more doubly heavy baryons is ongoing with little success [6].

Comprehensive theoretical literature has been developed exploring the physical properties of these heavy baryons using various techniques. These characteristics include their masses and residues [7–27], chiral effective Lagrangian [28], mixing angles [29], strong coupling constants [30–35], strong interactions and decays [36–39], radiative decays [17, 27, 33, 38, 40], weak decays [41–66], magnetic moments [67, 68], and lifetimes [69], *etc.* The computation of these properties requires the use of non-perturbative approaches. One such approach that has been successful and effective in calculating different hadronic parameters is the QCD sum rules, formulated by Shifman, Vainshtein, [70, 71], wherein correlation functions are examined via different interpolating currents [72–82].

Investigating polarization effects in heavy baryon decays provides a powerful mechanism for exploring the dynamics of weak interactions, revealing information that cannot be obtained from decay rates alone. We focus on the polarization structure of the decay $\Xi_{cc}^{++} \rightarrow \Xi_c^+ \bar{\ell} \nu_\ell$, which serves as a sensitive probe of the Lorentz covariant decomposition of the hadronic weak current [44]. Furthermore, these polarization measurements are particularly valuable for testing Standard Model (SM) predictions and potentially revealing signatures of new physics (NP) effects beyond the SM.

A lot of research over the past decades has focused on indirect signatures of new physics (NP) effects beyond the SM in the B physics sector [83–108]. In particular, one popular test of the SM has been measurement of the lepton flavor universality (LFU) ratios R_D and R_{D^*} [109–114]. It is to be noted that while these ratios have been of considerable curiosity with data pointing to anomalies of the order of $\sim 3\sigma$, further investigation has upheld the SM results to within 1.7σ . Nonetheless, such LFU ratios continue to play an important role as a test for the SM and in the hunt for NP signatures. We, therefore, also compute the LFU ratio for our process $\Xi_{cc}^{++} \rightarrow \Xi_c^+ \bar{\ell} \nu_\ell$.

We now comment on the structure of the rest of this manuscript. In Section 2, we describe the theoretical framework used to study the various physical observables of the decay $\Xi_{cc}^{++} \rightarrow \Xi_c^+ \bar{\ell} \nu_\ell$. We present the parameterization of the $\Xi_{cc}^{++} \rightarrow \Xi_c^+$ hadronic matrix elements in terms of form factors and use them to derive the branching ratio, forward-backward asymmetry, and polarization asymmetries. We also define and consider the corresponding polarization ratios. Section 3 begins with a listing of the numerical input parameters and the form factors. We then go on to examine the phenomenological implications through various observables of the decay $\Xi_{cc}^{++} \rightarrow \Xi_c^+ \bar{\ell} \nu_\ell$ in Section 3. Finally, we summarize our findings and present the conclusions in Section 4.

2 Theoretical Framework

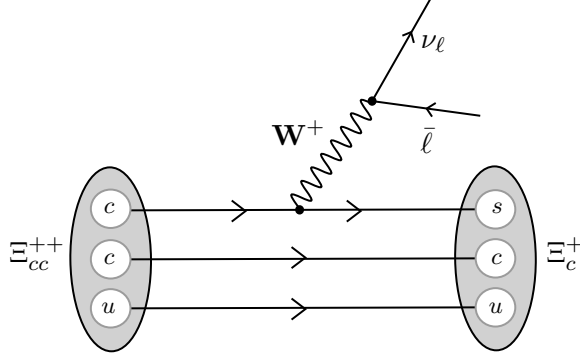


Figure 1. Feynman diagram for $\Xi_{cc}^{++} \rightarrow \Xi_c^+ \bar{\ell} \nu_\ell$ decay

The decay amplitude for this process can be written as:

$$\mathcal{A} = \frac{G_F}{\sqrt{2}} V_{cs}^* L^\mu \langle \Xi_c^+ | \bar{s} \gamma_\mu (1 - \gamma_5) c | \Xi_{cc}^{++} \rangle, \quad (2.1)$$

where $L^\mu = \bar{\nu}_\ell \gamma^\mu (1 - \gamma_5) \ell$ is the leptonic current, G_F is the Fermi constant, and V_{cs} is the relevant CKM matrix element.

The hadronic part, like the leptonic one, is the standard $V - A$ (vector – axial vector) interaction which can be parametrized in terms of six form factors consistent with the Lorentz structure [44]. The vector and axial vector currents become,

$$\begin{aligned} \langle \Xi_c^+(p', s') | V^\mu | \Xi_{cc}^{++}(p, s) \rangle &= \bar{u}_{\Xi_c^+}(p', s') \left[\mathcal{F}_1(q^2) \gamma^\mu + \mathcal{F}_2(q^2) \frac{p^\mu}{M_{\Xi_{cc}^{++}}} + \mathcal{F}_3(q^2) \frac{p'^\mu}{M_{\Xi_c^+}} \right] u_{\Xi_{cc}^{++}}(p, s), \\ \langle \Xi_c^+(p', s') | A^\mu | \Xi_{cc}^{++}(p, s) \rangle &= \bar{u}_{\Xi_c^+}(p', s') \left[\mathcal{G}_1(q^2) \gamma^\mu + \mathcal{G}_2(q^2) \frac{p^\mu}{M_{\Xi_{cc}^{++}}} + \mathcal{G}_3(q^2) \frac{p'^\mu}{M_{\Xi_c^+}} \right] \gamma_5 u_{\Xi_{cc}^{++}}(p, s), \end{aligned}$$

where $\mathcal{F}_1(q^2)$, $\mathcal{F}_2(q^2)$, and $\mathcal{F}_3(q^2)$ are the form factors for the vector current while $\mathcal{G}_1(q^2)$, $\mathcal{G}_2(q^2)$ and $\mathcal{G}_3(q^2)$ are the form factors for the axial vector current.

In order to be able to discuss the polarization characteristics of the particles involved in the decay $\Xi_{cc}^{++} \rightarrow \Xi_c^+ \bar{\ell} \nu_\ell$, we define mutually orthogonal spin projection vectors via,

$$\hat{e}_L = \frac{\vec{p}_m}{|\vec{p}_m|}, \quad \hat{e}_N = \frac{\vec{k}_r \times \vec{p}_m}{|\vec{k}_r \times \vec{p}_m|}, \quad \hat{e}_T = \hat{e}_N \times \hat{e}_L. \quad (2.2)$$

Here \vec{p}_m is the momentum of the particle m under consideration ($m = \Xi_{cc}^{++}, \Xi_c^+, \bar{\ell}$), and \vec{k}_r provides a reference direction to be able to define the normal to the plane of \vec{p}_m and \vec{k}_r . While discussing the polarization of $\bar{\ell}$, we take the momentum of Ξ_{cc}^{++} as the reference. In the case of a discussion of the polarization of either baryon, the momentum of $\bar{\ell}$ provides the reference direction. The labels L, N, T are used for the longitudinal, normal and transverse directions, respectively. It is convenient to imagine these directions as belonging to the ‘rest

frame' of the particle under consideration. When boosted to the center of mass frame, the longitudinal polarization four-vector transforms to:

$$S_{L,\text{CM}}^\mu = \left(\frac{|\vec{p}_m|}{M_m}, \frac{E_m \vec{p}_m}{M_m |\vec{p}_m|} \right), \quad (2.3)$$

while the normal and transverse remain unchanged. Here M_m is the mass of particle m and E_m is its energy. To obtain the polarization structure, we apply the spin projector $\frac{1}{2}(1 + \gamma_5 \not{S})$ on the baryonic and leptonic tensors by making the replacement $(\not{p}_m + M_m) \rightarrow (\not{p}_m + M_m) \frac{1}{2}(1 + \gamma_5 \not{S})$.

The polarization structure of the decay is given by the differential branching ratio,

$$\begin{aligned} \mathcal{D}_k^{(m,n)}(q^2, \cos \theta) &\equiv \frac{d^2 \tilde{\mathcal{D}}_k^{(m,n)}(q^2, \cos \theta)}{dq^2 d(\cos \theta)}, \\ &= \frac{G_F^2 |V_{cs}|^2 \tau_{\Xi_{cc}^{++}}}{2} \frac{q^2 \sqrt{Q_+ Q_-}}{2 M_{\Xi_{cc}^{++}}} \left(1 - \frac{m_\ell^2}{q^2}\right)^2 |\mathcal{A}_k^{(m,n)}(q^2, \cos \theta)|^2, \end{aligned} \quad (2.4)$$

where $Q_+ = (M_{\Xi_{cc}^{++}} + M_{\Xi_c^+})^2 - q^2$ and $Q_- = (M_{\Xi_{cc}^{++}} - M_{\Xi_c^+})^2 - q^2$. The index k takes on the values \pm referring to the polarization of particle m ($m \in \{\ell, \Xi_{cc}^{++}, \Xi_c^+\}$) in the direction n ($n \in \{L, T\}$). Note that we only consider the results with one particle polarized at a time and also discuss the unpolarized branching ratio result using the symbol \mathcal{D} for it. Further, note the conspicuous absence of the normal direction N in which we find a zero branching fraction. The expression for the squared amplitude $|\mathcal{A}_k^{(m,n)}|^2$, after integrating over $\cos \theta$, for the case of polarized particles is presented in Appendix B while the unpolarized case yields the result,

$$\begin{aligned} |\mathcal{A}|^2 &= \frac{8}{3q^4} (q^2 - m_\mu^2) \left\{ 24q^4 M_{\Xi_c^+} M_{\Xi_{cc}^{++}} (-\mathcal{F}_1^2 + \mathcal{G}_2^2) + 4(\mathcal{F}_1^2 + \mathcal{G}_2^2) [q^4 (M_{\Xi_c^+}^2 + M_{\Xi_{cc}^{++}}^2 - m_\mu^2) \right. \\ &\quad - m_\mu^2 q^2 (M_{\Xi_c^+}^2 + M_{\Xi_{cc}^{++}}^2) + (2m_\mu^2 + q^2)(M_{\Xi_c^+}^2 - M_{\Xi_{cc}^{++}}^2)^2 - 2q^6] + \frac{1}{M_{\Xi_{cc}^{++}}^2} \left[(M_{\Xi_c^+}^2 \right. \\ &\quad - M_{\Xi_{cc}^{++}}^2)^2 - 2M_{\Xi_c^+}^2 q^2 + q^4] (2m_\mu^2 + q^2) - 2M_{\Xi_{cc}^{++}}^2 q^2 (q^2 - m_\mu^2) \left. \right] \left[Q_+ \mathcal{F}_2^2 + Q_- \mathcal{G}_2^2 \right] \\ &\quad + \frac{1}{M_{\Xi_c^+}^2} \left[(M_{\Xi_c^+}^2 - M_{\Xi_{cc}^{++}}^2)^2 - 2M_{\Xi_{cc}^{++}}^2 q^2 + q^4 \right] (2m_\mu^2 + q^2) - 2M_{\Xi_c^+}^2 q^2 (q^2 - m_\mu^2) \left. \right] \left[Q_+ \mathcal{F}_3^2 \right. \\ &\quad + Q_- \mathcal{G}_3^2 \left. \right] + 4Q_+ \mathcal{F}_1 \left[\left(\frac{\mathcal{F}_2}{M_{\Xi_{cc}^{++}}} + \frac{\mathcal{F}_3}{M_{\Xi_c^+}} \right) ((M_{\Xi_c^+} - M_{\Xi_{cc}^{++}})^2 (2m_\mu^2 + q^2) - q^4) (M_{\Xi_c^+} \right. \\ &\quad + M_{\Xi_{cc}^{++}}) + m_\mu^2 q^2 \left[\frac{\mathcal{F}_2}{M_{\Xi_{cc}^{++}}} (M_{\Xi_{cc}^{++}} - 2M_{\Xi_c^+}) + \frac{\mathcal{F}_3}{M_{\Xi_c^+}} (M_{\Xi_c^+} - 2M_{\Xi_{cc}^{++}}) \right] \left. \right] + 4Q_- \mathcal{G}_2 \\ &\quad \times \left[\left(-\frac{\mathcal{G}_2}{M_{\Xi_{cc}^{++}}} + \frac{\mathcal{G}_3}{M_{\Xi_c^+}} \right) ((M_{\Xi_c^+} + M_{\Xi_{cc}^{++}})^2 (2m_\mu^2 + q^2) - q^4) (M_{\Xi_c^+} - M_{\Xi_{cc}^{++}}) + m_\mu^2 q^2 \right. \\ &\quad \times \left. \left[-\frac{\mathcal{G}_2}{M_{\Xi_{cc}^{++}}} (M_{\Xi_{cc}^{++}} + 2M_{\Xi_c^+}) + \frac{\mathcal{G}_3}{M_{\Xi_c^+}} (M_{\Xi_c^+} + 2M_{\Xi_{cc}^{++}}) \right] \right] + \frac{2}{M_{\Xi_c^+} M_{\Xi_{cc}^{++}}} \left[-q^4 \left[2(M_{\Xi_c^+}^2 \right. \right. \end{aligned}$$

$$\begin{aligned}
& + M_{\Xi_{cc}^{++}}^2 + m_\mu^2 \Big] + (2m_\mu^2 + q^2)(M_{\Xi_c^+}^2 - M_{\Xi_{cc}^{++}}^2)^2 - m_\mu^2 q^2 (M_{\Xi_c^+}^2 + M_{\Xi_{cc}^{++}}^2) + q^6 \Big] \left[Q_+ \mathcal{F}_2 \mathcal{F}_3 \right. \\
& \left. + Q_- \mathcal{G}_2 \mathcal{G}_3 \right] \Big\}. \tag{2.5}
\end{aligned}$$

The forward-backward asymmetry (FBA) is defined as,

$$\text{FBA}_k^{(m,n)}(q^2) = \frac{\mathcal{N}_k^{F(m,n)} - \mathcal{N}_k^{B(m,n)}}{\mathcal{N}_k^{F(m,n)} + \mathcal{N}_k^{B(m,n)}}, \tag{2.6}$$

where $\mathcal{N}_k^{F(m,n)}$ ($\mathcal{N}_k^{B(m,n)}$) is the probability of the lepton $\ell = \mu$ moving in the forward (backward) direction. In terms of the differential decay rate, these probabilities can be computed using,

$$\mathcal{N}_k^{F(m,n)}(q^2) = \int_0^1 d(\cos \theta) \mathcal{D}_k^{(m,n)}(q^2, \cos \theta), \quad \mathcal{N}_k^{B(m,n)}(q^2) = \int_{-1}^0 d(\cos \theta) \mathcal{D}_k^{(m,n)}(q^2, \cos \theta). \tag{2.7}$$

It is useful to study the polarization asymmetries $P^{(m,n)}$ defined via,

$$P^{(m,n)}(q^2) = \frac{\int_{-1}^1 d(\cos \theta) \mathcal{D}_+^{(m,n)}(q^2, \cos \theta) - \int_{-1}^1 d(\cos \theta) \mathcal{D}_-^{(m,n)}(q^2, \cos \theta)}{\int_{-1}^1 d(\cos \theta) \mathcal{D}_+^{(m,n)}(q^2, \cos \theta) + \int_{-1}^1 d(\cos \theta) \mathcal{D}_-^{(m,n)}(q^2, \cos \theta)}. \tag{2.8}$$

The $P^{(m,n)}$ address the question of the asymmetry in the polarization of particle m in the direction n by computing a measure for the asymmetry *vis a vis* the positive and negative helicity state as a function of q^2 . We go on to also compute the q^2 -averaged values of the $P^{(m,n)}$.

We also consider and define the ratios for the polarizations of the parent baryon Ξ_{cc}^{++} , the daughter baryon Ξ_c^+ , and the muon ℓ , defined via the following expression:

$$\mathcal{R}_{nn'}^{(m,m')}[j] \equiv \frac{\int_{-1}^1 d(\cos \theta) \mathcal{D}_j^{(m,n)}(q^2, \cos \theta)}{\int_{-1}^1 d(\cos \theta) \mathcal{D}_j^{(m',n')}(q^2, \cos \theta)}, \tag{2.9}$$

where $j = \pm$ refers to the polarization¹. The ratio $\mathcal{R}_{nn'}^{(m,m')}[j]$ provides a measure for comparing the ‘numbers’ of m -type particles polarized with helicity j in the n direction with the m' -type particles polarized with helicity j in the n' direction. It turns out that we can define polarization asymmetry ratios building on Eq. 2.9 that may be more robust against form factor uncertainties:

$$\mathcal{R}_{P^{(m,m')}} \equiv \frac{\mathcal{R}_{nn'}^{(m,m')}[+] - \mathcal{R}_{nn'}^{(m,m')}[-]}{\mathcal{R}_{nn'}^{(m,m')}[+] + \mathcal{R}_{nn'}^{(m,m')}[-]}. \tag{2.10}$$

¹One may argue that a more general ratio, for example $\mathcal{R}_{TL}^{(\Xi_{cc}^{++}, \ell)}[j, k] \equiv \mathcal{D}_j^{(\Xi_{cc}^{++}, T)} / \mathcal{D}_k^{(\ell, L)}$, could be considered. We did try looking at such quantities but found the description too cumbersome without any clear phenomenological advantage and, therefore, chose to settle with the simpler quantities with $j = k$.

3 Phenomenological study

3.1 Input parameters

We show, in Table 1, various parameters (masses, Fermi constant, the relevant CKM matrix element and lifetime of the Ξ_{cc}^{++}) used in our analysis [115]. We note that we have used the central values given in Table 1.

$m_c = (1.27 \pm 0.02) \text{ GeV}$	$m_e = 0.51 \text{ MeV}$	$m_\mu = 105 \text{ MeV}$
$M_{\Xi_{cc}^{++}} = (3.62 \pm 0.0015) \text{ GeV}$	$M_{\Xi_c^+} = (2.46 \pm 0.00023) \text{ GeV}$	$G_F = 1.17 \times 10^{-5} \text{ GeV}^{-2}$
$ V_{sc} = (0.974 \pm 0.006)$	$\tau_{\Xi_{cc}^{++}} = (2.56 \pm 0.27) \times 10^{-13} \text{ s}$	

Table 1. Numerical values of various input parameters used in numerical analysis [115].

The hadronization of quarks and gluons is described in terms of form factors that are a source of theoretical uncertainties. The form factors that we use for $\Xi_{cc}^{++} \rightarrow \Xi_c^+$ are computed using QCD sum rules and taken from K. Azizi *et al* [44], with

$$F(q^2) = \frac{F(0)}{\left(1 - \alpha_1 \left(\frac{q}{M_{\Xi_{cc}^{++}}}\right)^2 + \alpha_2 \left(\frac{q}{M_{\Xi_{cc}^{++}}}\right)^4 + \alpha_3 \left(\frac{q}{M_{\Xi_{cc}^{++}}}\right)^6 + \alpha_4 \left(\frac{q}{M_{\Xi_{cc}^{++}}}\right)^8\right)}, \quad (3.1)$$

describing the q^2 (momentum transfer) dependence of the form factors \mathcal{F}_i and \mathcal{G}_i . The values of $F(0)$, α_1 , α_2 , α_3 and α_4 corresponding to the various form factors are given in Table 2.

	\mathcal{F}_1	\mathcal{F}_2	\mathcal{F}_3	\mathcal{G}_1	\mathcal{G}_2	\mathcal{G}_3
$F(0)$	-0.37 ± 0.13	1.35 ± 0.43	0.16 ± 0.06	0.20 ± 0.06	1.34 ± 0.43	-1.86 ± 0.65
α_1	1.54	-0.05	1.99	2.79	1.07	2.15
α_2	-23.84	-111.38	17.17	35.82	-78.83	-27.91
α_3	268.50	1329.88	-442.35	-541.92	935.73	449.20
α_4	-1174.79	-5206.92	2372.78	2240.25	-3550.64	-2702.99

Table 2. Form factors of $\Xi_{cc}^{++} \rightarrow \Xi_c^+$ decays which are calculated using QCD sum rules [44]

3.2 Observables focusing on one particle at a time

In this section, we present the phenomenological analysis of various unpolarized and polarized observables from the corresponding differential decay distributions that focus on one particle at a time. In particular, we discuss the branching ratio $\mathcal{D}_k^{(m,n)}$, forward backward asymmetry $\text{FBA}_k^{(m,n)}$, and polarization asymmetries $P^{(m,n)}$. We have used a consistent color scheme for all the figures: black is used for the unpolarized results, green corresponds to the $k = +$ polarized state, and red denotes the $k = -$ polarized state. We use dashed lines to indicate the form factor uncertainties.

3.2.1 Polarized (m, n) cases

We begin presenting our results by discussing the branching ratio $\mathcal{D}_k^{(m,L)}$ and $\text{FBA}_k^{(m,L)}$ as a function of q^2 for the cases of $m \in \{\Xi_{cc}^{++}, \Xi_c^+, \mu^+\}$ with the longitudinal direction chosen for polarization. As described earlier, the case of $k = +$ is presented in green and $k = -$ in red with the unpolarized result in black.

In Fig. 2a, we present the branching ratio for the longitudinal direction in the case of the muon. The peak height and position of the green and black curves are effectively the same, while the red curve is an order of magnitude lower exhibiting a clear hierarchy $\mathcal{D}(q^2) \sim \mathcal{D}_+^{(\ell,L)}(q^2) \gg \mathcal{D}_-^{(\ell,L)}(q^2)$. Near the endpoint of the distribution, the projector continues to favor $k = +$, while the $k = -$ rate is suppressed due to kinematic and spin effects².

In Fig. 2b, we show the forward-backward asymmetry $\text{FBA}_k^{(\ell,L)}$ as a function of q^2 . It can be seen that for the case of the muon, the longitudinal polarization effects are quite distinct from each other in the low q^2 bin but do decrease towards the high q^2 bin. Since the branching ratio $\mathcal{D}(q^2) \sim \mathcal{D}_+^{(\ell,L)}(q^2)$, the forward-backward asymmetry in the unpolarized (black) case generally tracks the $k = +$ (green) case except in the low q^2 region where the branching ratio is small overall and there is a large forward-backward asymmetry in the $k = -$ (red) state. The black curve exhibits a zero crossing at $q^2 \sim 0.9 \text{ GeV}^2$, while the red (green) curve remains negative (positive) throughout the full range of q^2 .

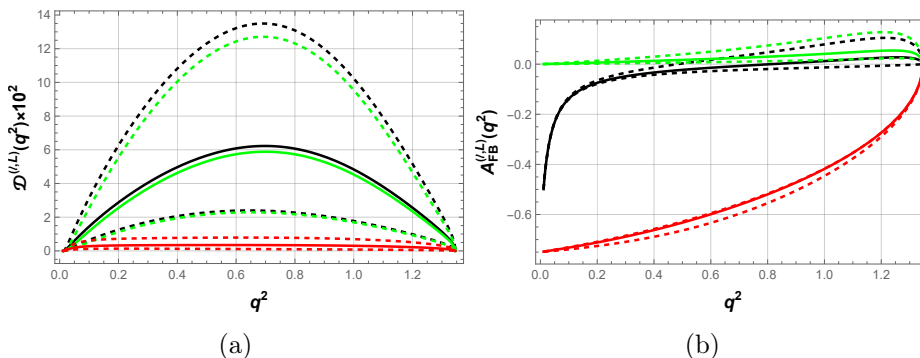


Figure 2. Differential branching ratios $\mathcal{D}_k^{(m,n)}(q^2)$, integrated over $\cos \theta$, and forward-backward asymmetry $\text{FBA}_k^{(m,n)}(q^2)$ as functions of q^2 for the SM unpolarized (black) and the longitudinally (L) polarized muon (ℓ) cases. The $k = +$ longitudinally polarized state is in green and the $k = -$ one is in red. The dotted region represents uncertainty due to form factors.

In Fig. 3a, we examine the case of the longitudinally polarized daughter baryon Ξ_c^+ . The corresponding observable is $\mathcal{D}_k^{(\Xi_c^+,L)}(q^2)$. We observe that the Ξ_c^+ is predominantly produced in the $k = -$ (red) state, while the $k = +$ (green) state is strongly suppressed. Most of the total BR comes from the $k = -$ state. In Fig. 3b, we show the $\text{FBA}_k^{(\Xi_c^+,L)}(q^2)$. At low q^2 , near the threshold, the curve starts at negative values for the unpolarized as well as the polarized cases. The forward-backward asymmetry increases in the low q^2 region with

²This suppression of the $k = -$ state relative to the $k = +$ state at the end-point of the distribution is not obvious in Fig. 2a

both the $k = +$ longitudinally polarized (green) as well as the unpolarized (black) values exhibiting a zero crossing. In particular, at large q^2 , the $k = +$ longitudinally polarized Ξ_c^+ particle exhibits a large forward-backward asymmetry. Since the decay is predominantly into the $k = -$ state, the unpolarized forward-backward asymmetry mostly tracks this state for most of the dynamical range ($q^2 \lesssim 1.0 \text{ GeV}^2$). Overall, the Ξ_c^+ with $k = +$ (green) favors the forward direction, while $k = -$ (red) maintains a backward tendency. Near q_{max}^2 , the green curve rises peaks giving a forward-backward asymmetry ~ 0.62 , whereas the red curve drops to a negative value ~ -0.5 .

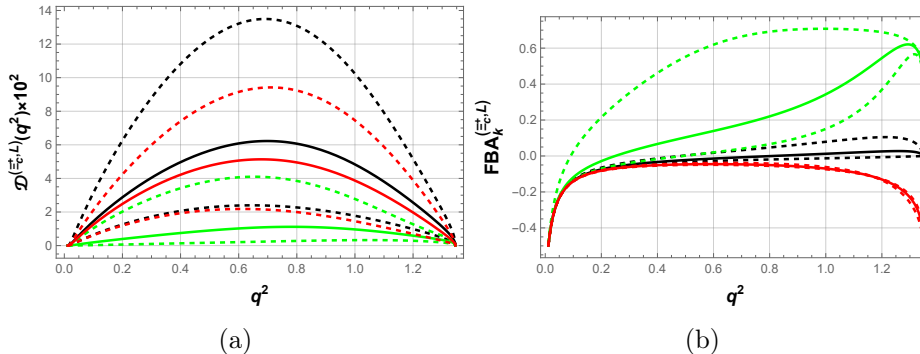


Figure 3. Differential branching ratios $\mathcal{D}_k^{(m,n)}(q^2)$, integrated over $\cos\theta$, and forward-backward asymmetry $\text{FBA}_k^{(m,n)}(q^2)$ as functions of q^2 for the SM unpolarized (black) and the longitudinally (L) polarized daughter baryon Ξ_c^+ cases. Color coding is the same as in Fig. 2.

In Fig. 4a, the parent baryon Ξ_{cc}^{++} is longitudinally polarized, and we probe the effect of the longitudinal spin orientation of the initial state on the decay dynamics. The hierarchy follows the pattern $\mathcal{D}^{(\Xi_{cc}^{++},L)}$ (black) $\gtrsim \mathcal{D}_-^{(\Xi_{cc}^{++},L)}$ (red) $\gg \mathcal{D}_+^{(\Xi_{cc}^{++},L)}$ (green), with the maximum of the green curve ($k = +$) an order of magnitude smaller than the maximum of the red ($k = -$). In Fig. 4b, we present $\text{FBA}_k^{(\Xi_{cc}^{++},L)}$ as function of the momentum transfer. There is a zero crossing at $q^2 \sim 0.5 \text{ GeV}^2$ for the black (unpolarized) and red ($k = -$) curves, whereas the green ($k = +$) curve remains negative. Since the decay amplitude for the $k = -$ state is much larger than the $k = +$ state, the forward-backward asymmetry for the unpolarized case mainly tracks the red ($k = -$) curve. The distinction between the two polarization states is obvious in the high q^2 bin, which forces the unpolarized (black) forward-backward asymmetry to deviate somewhat from the red ($k = -$) curve. At low q^2 , we observe a strong overall backward preference.

We now move on to present the differential branching ratio and the forward-backward asymmetry for the case of transversely polarized ($n = T$) particles. In Fig. 5a, we can see that for the transverse polarized muon, the hierarchy at all q^2 is $\mathcal{D}(q^2)$ (black) $> \mathcal{D}_-^{(\ell,T)}(q^2)$ (red) $> \mathcal{D}_+^{(\ell,T)}(q^2)$ (green). The $\text{FBA}_k^{(\ell,T)}(q^2)$ for the transverse polarized muon presented in Fig. 5b clearly shows the distinction between the $k = +$ state (green) as having a forward preference with the $k = -$ (red) having a backward one. The unpolarized forward-backward asymmetry sits between the two and shows very little forward-backward asymmetry in the mid to large q^2 regime. At low q^2 , all curves start negative, but the green

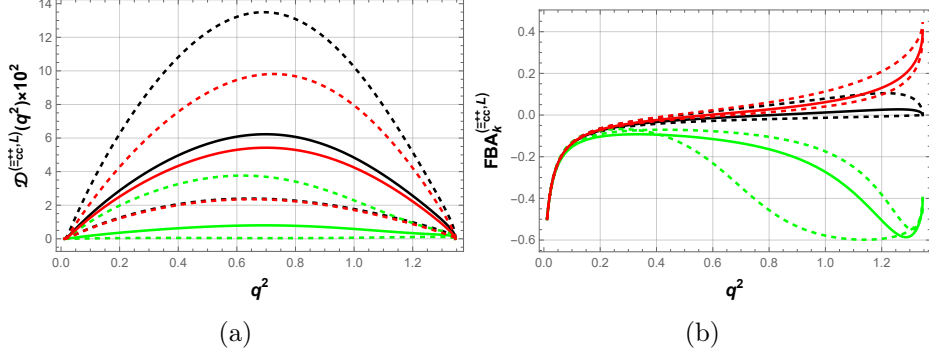


Figure 4. Differential branching ratios $\mathcal{D}_k^{(m,n)}(q^2)$, integrated over $\cos\theta$, and forward–backward asymmetry $\text{FBA}_k^{(m,n)}(q^2)$, integrated over $\cos\theta$, as functions of q^2 for the SM unpolarized (black) and the longitudinally (L) polarized parent baryon Ξ_{cc}^{++} cases. Color coding is the same as in Fig. 2.

one ($k = +$) increases rapidly and becomes positive (~ 0.01 GeV) almost immediately. The unpolarized forward-backward asymmetry is more influenced by the $k = -$ (red) state.

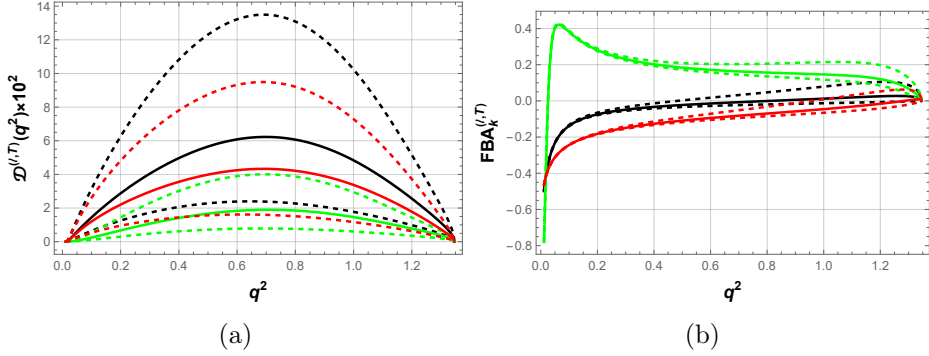


Figure 5. Differential branching ratios $\mathcal{D}_k^{(m,n)}(q^2)$, integrated over $\cos\theta$, and forward–backward asymmetry $\text{FBA}_k^{(m,n)}(q^2)$, integrated over $\cos\theta$, as functions of q^2 for the SM unpolarized and the transversely (T) polarized muon ℓ cases. Color coding is the same as in Fig. 2.

In Fig. 6a and Fig. 6b, we present the branching ratio and the forward-backward asymmetry for the case of the transverse polarized Ξ_c^+ , respectively. We can see that the splitting between the branching ratio in the $k = +$ (green) and $k = -$ (red) states is modest in the low and high q^2 regions, and peaks for the mid q^2 allowed region. The transverse daughter-spin projection reveals a slight polarization preference with the Ξ_c^+ being produced more frequently in the spin $+1/2$ ($k = +$) state. The $\text{FBA}_k^{(\Xi_c^+, T)}(q^2)$ reveals that the $k = -$ (red) transverse polarized daughter Ξ_c^+ has a clear backward tendency as opposed to the $k = +$ (green) state. The unpolarized $\text{FBA}_k^{(\Xi_c^+, T)}(q^2)$ resultantly hovers around the zero mark for most of the q^2 region.

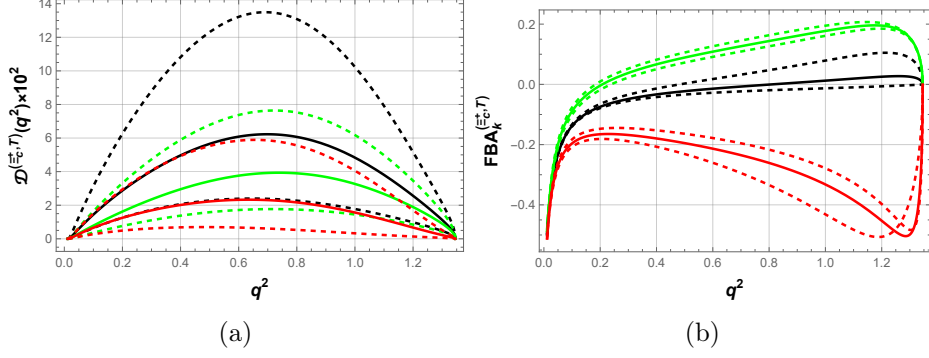


Figure 6. Differential branching ratios $\mathcal{D}_k^{(m,n)}(q^2)$, integrated over $\cos\theta$, and forward–backward asymmetry $\text{FBA}_k^{(m,n)}(q^2)$, integrated over $\cos\theta$, as functions of q^2 for the SM unpolarized and the transversely (T) polarized daughter Ξ_c^+ cases. Color coding is the same as in Fig. 2.

In Fig. 7a and Fig. 7b, we finally consider the transverse polarization effects of the Ξ_{cc}^{++} . It can be seen that throughout the dynamical range, $\mathcal{D}(q^2)$ (black) $>$ $\mathcal{D}_-^{(\Xi_{cc}^{++},T)}(q^2)$ (red) \sim $\mathcal{D}_+^{(\Xi_{cc}^{++},T)}(q^2)$ (green). At higher $q^2 \gtrsim 0.5 \text{ GeV}^2$, we can see a somewhat higher value for $\mathcal{D}_-^{(\Xi_{cc}^{++},T)}(q^2)$ (red) as compared with $\mathcal{D}_+^{(\Xi_{cc}^{++},T)}(q^2)$ (green). In Fig. 7b, we can see that $\text{FBA}_k^{(\Xi_{cc}^{++},T)}(q^2)$ starts off as negative. However, for $q^2 \gtrsim 0.2 \text{ GeV}^2$, the $k = +$ (green) polarized Ξ_{cc}^{++} shows a positive forward-backward asymmetry while the $k = -$ state continues to prefer the backward direction. Given that the branching ratios of the two states are similar, we can correspondingly see very little forward-backward asymmetry in the unpolarized case for the Ξ_{cc}^{++} .

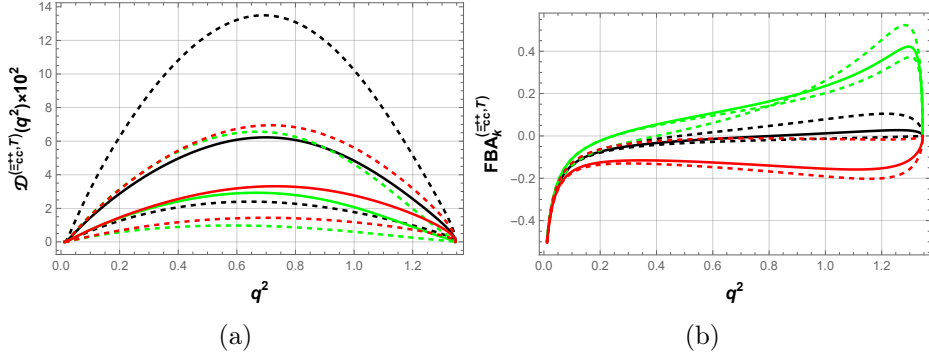


Figure 7. Differential branching ratios $\mathcal{D}_k^{(m,n)}(q^2)$, integrated over $\cos\theta$, and forward–backward asymmetry $\text{FBA}_k^{(m,n)}(q^2)$, integrated over $\cos\theta$, as functions of q^2 for the SM unpolarized and the transversely (T) polarized parent Ξ_{cc}^{++} cases. Color coding is the same as in Fig. 2.

The variations due to form factor uncertainties in the binned branching ratios and forward-backward asymmetry for each case are respectively shown in the left and right panels of Fig. 8. The available q^2 range in Fig. 8 is divided into four bins: low $q^2 \in [0.0112, 0.4] \text{ GeV}^2$ (row 2), mid $q^2 \in [0.4, 0.8] \text{ GeV}^2$ (row 3), high $q^2 \in [0.8, 1.346] \text{ GeV}^2$ (row 4), with the fourth bin corresponding to the whole dynamical range $q^2 \in [0.0112, 1.346] \text{ GeV}^2$ (row 1).

For each polarization state ($k = 0, +, -$), the quantity $\mathcal{D}_k^{(m,n)}(q^2)$ ($\text{FBA}_k^{(m,n)}(q^2)$) is integrated over each bin via $\int_{\text{bin}} dq^2 \mathcal{D}_k^{(m,n)}(q^2) / \int_{\text{bin}} dq^2$ ($\int_{\text{bin}} dq^2 \text{FBA}_k^{(m,n)}(q^2) / \int_{\text{bin}} dq^2$). The error bars for each bin are colored-coded the same way as earlier stated, with black, green, and red, corresponding to the bin averaged values of $\mathcal{D}^{(m,n)}(q^2)$, $\mathcal{D}_+^{(m,n)}(q^2)$, and $\mathcal{D}_-^{(m,n)}(q^2)$ ($\text{FBA}^{(m,n)}(q^2)$, $\text{FBA}_+^{(m,n)}(q^2)$, and $\text{FBA}_-^{(m,n)}(q^2)$), respectively. The blue asterisk in each graph is the central value of the respective observable. The values for both branching ratios and forward-backward asymmetry for each bin are mentioned in Table 3, 4, 5, and 6 in Appendix A.

Generally, the branching ratios $\mathcal{D}_k^{(m,n)}$ show a larger magnitude variation in the mid q^2 [0.4-0.8] GeV² (row 3) and high q^2 [0.8-1.346] GeV² (row 4) bins, shown in Figs. 8e and 8g respectively, than in the low q^2 [0.0112-0.4] GeV² bin, shown in Fig. 8c. The exception to this behavior is the negatively polarized muon ℓ in the longitudinal direction, where the variation across all bins is roughly the same.

The effect of the form factor uncertainties on the forward-backward asymmetry $\text{FBA}_k^{(m,n)}$ for each m, n case is less apparent compared to that on their respective branching ratios, as shown on the right panels of Fig. 8. However, that is not the case for the positively polarized daughter baryon Ξ_c^+ and parent baryon Ξ_{cc}^{++} in the longitudinal direction where the error bars are significant in each bin.

While for most cases the particular combination of form factor uncertainties chosen resulted in their central value lying within their variation, the one for the positively polarized parent baryon Ξ_{cc}^{++} in the transverse direction is beyond the variation shown in Fig. 8b. This is because the ‘upper’ and ‘lower’ limits of all the FBA_k plots just correspond respectively to the results obtained after considering the upper and lower values of the form factors shown in Table 2. This only gives an idea of the order of magnitude of the uncertainty caused by the form factors as there are interference effects in the amplitude. As a result, the true variation in the branching ratio, as well as the FBA_k as a result of form factor uncertainties is expected to be larger than the ones shown in Fig. 8.

In order to analyze this properly, we did an exhaustive computation of uncertainties caused by form factors and present our results for one special case in Fig. 9. In Fig. 9, the true uncertainty envelope for the forward backward asymmetry due to form factors is shown as shaded green (for the $k = +$ transverse polarized parent baryon) and red (for the $k = -$ transverse polarized parent baryon) regions. We also show, as dotted lines, the uncertainty regions that were obtained for the same observable in Fig. 7b. This analysis confirms the interference effects in the amplitude and show that the expected picture emerges once all uncertainties are accounted for correctly.

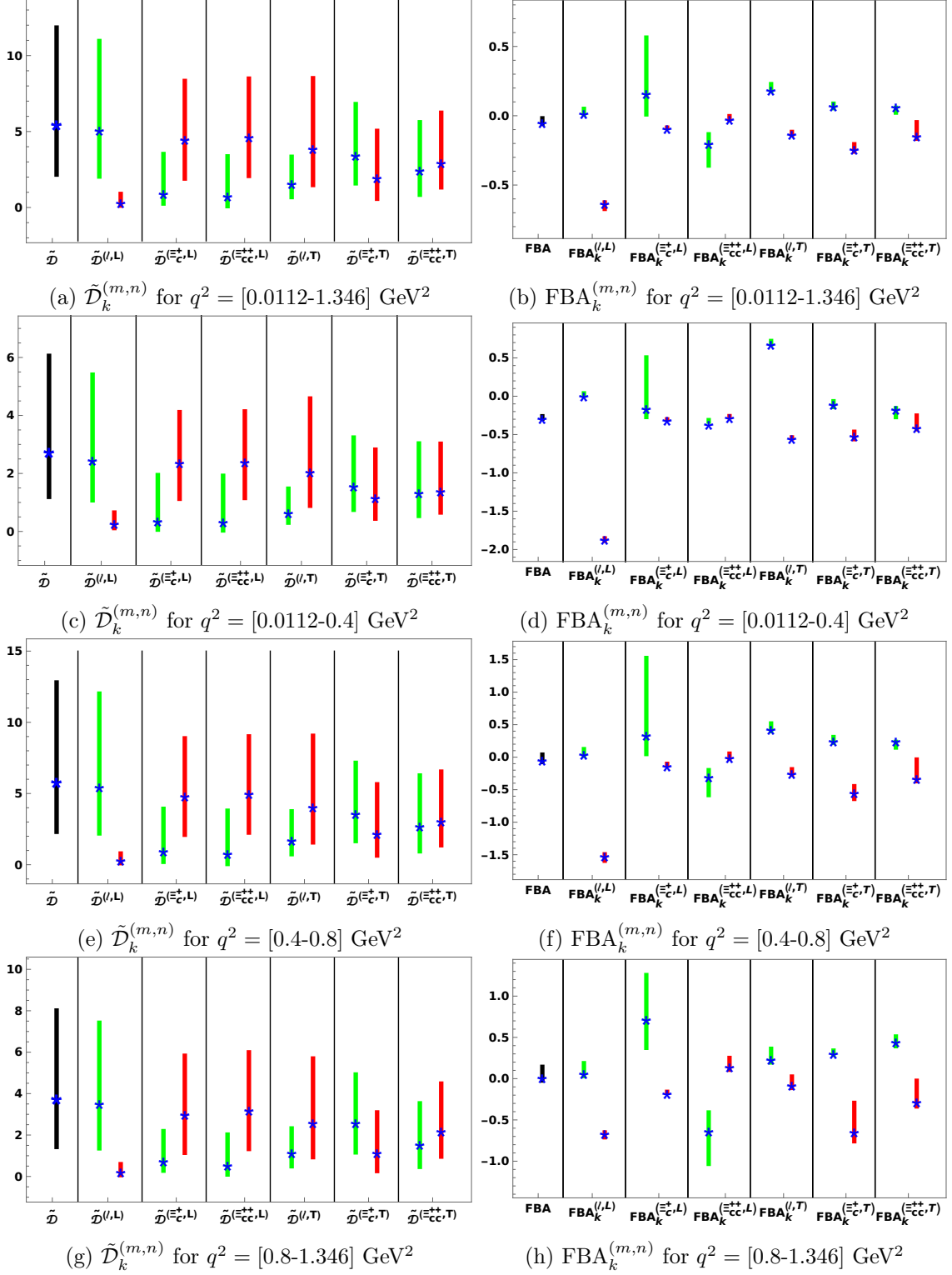


Figure 8. Variation in the magnitudes of the branching ratio $\tilde{D}_k^{(m,n)}$ and the forward-backward asymmetry $\text{FBA}_k^{(m,n)}$ shown in left and right panels, respectively, after integrating over four different q^2 bins: $[0.0112-1.346]$ GeV² in Figs. 8a and 8b, $[0.0112-0.4]$ GeV² in Figs. 8c and 8d, $[0.4-0.8]$ GeV² in Figs. 8e and 8f, and $[0.8-1.346]$ GeV² in Figs. 8g and 8h. The blue asterisk ‘*’ marks the central value of the branching ratio or the forward-backward asymmetry in the respective bins.

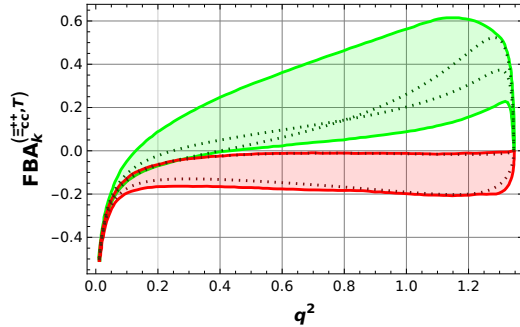


Figure 9. A detailed analysis of the form factor uncertainty of the forward-backward asymmetry $FBA_k^{m,n}(q^2)$, integrated over $\cos\theta$, of the transversely (T) polarized parent baryon Ξ_{cc}^{++} as a function of q^2 , obtained by varying form factor uncertainties within their $\pm 1\sigma$ allowed regions. The green envelope indicates the total variation by the positive polarization, whereas the red envelope indicates that by the negative one. The dotted dark green and dark red lines correspond to the uncertainty reported in Fig. 7b.

3.3 Lepton-Flavor Universality

The SM is based on a lepton-flavor universal structure of the gauge interactions, and recent measurements of lepton-flavor universality in \mathcal{R}_{K^*} are consistent with SM predictions. However, anomalies have been reported in the $\mathcal{R}_{D^{(*)}}$ [114]. At any rate, the lepton flavor universality ratios provide a robust test of the SM. We have also calculated the LFU ratio, defined via $\mathcal{R}_{\Xi_c^+}(\mu/e) \equiv \mathcal{D}(\Xi_{cc}^{++} \rightarrow \Xi_c^+ \mu^+ \nu_\mu) / \mathcal{D}(\Xi_{cc}^{++} \rightarrow \Xi_c^+ e^+ \nu_e)$. The result of this LFU ratio across the entire q^2 range is shown in Fig. 10. By averaging over the entire q^2 region, we obtain the value $\mathcal{R}_{\Xi_c^+}(\mu/e) = 1.00229^{+0.00374}_{-0.01551}$. It is also interesting to note that $\mathcal{R}_{\Xi_c^+}(\mu/e)$ has the values $0.942998^{+0.002094}_{-0.008187}$, $1.00224^{+0.00296}_{-0.01069}$, $1.03615^{+0.00710}_{-0.02149}$ in the low, mid and high q^2 regions, respectively.

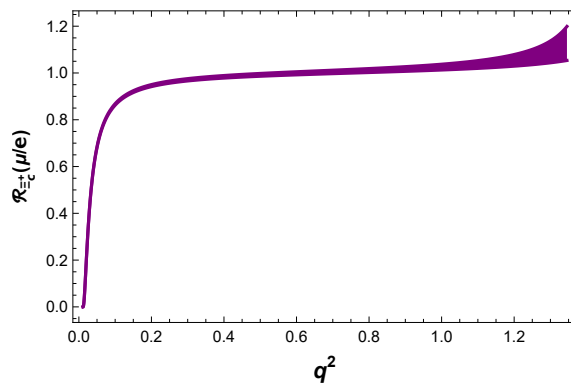


Figure 10. The lepton flavor universality ratio $\mathcal{R}_{\Xi_c^+}(\mu/e)$ as a function of q^2 .

3.4 Polarization Asymmetry Analysis

We now focus our attention to an analysis of the polarization asymmetry in the decay $\Xi_{cc}^{++} \rightarrow \Xi_c^+ \bar{\ell} \nu_\ell$. We describe the polarization asymmetry $P^{(m,n)}$, the polarization ratio

$\mathcal{R}_{nn'}^{(m,m')}[j]$, and the polarization asymmetry ratio $\mathcal{R}_{P_{nn'}^{(m,m')}}$ as defined in Eq. 2.8, Eq. 2.9, and Eq. 2.10, respectively.

3.4.1 Polarization Asymmetry $P^{(m,n)}$

In this section, we analyze the spin polarization asymmetries $P^{(m,n)}$ by plotting those as functions of q^2 in Figs. 11 and 12. The $P^{(m,n)}$ quantifies the differences in the branching ratios (after integrating over $\cos\theta$) of the positive ($k = +$) and negative ($k = -$) polarization states of the particle m ($m \in \{\ell, \Xi_{cc}^{++}, \Xi_c^+\}$) in the n ($n \in \{L, T\}$) direction. The brown curve represents the central value of $P^{(m,n)}$, while the dotted curves indicate variation due to uncertainties in the form factors.

In Fig. 11, we present the spin polarization asymmetries $P^{(m,L)}$ for the longitudinally polarized muon ℓ , daughter baryon Ξ_c^+ , and parent baryon Ξ_{cc}^{++} . For the muon, Fig. 11a shows that the observable $P^{(\ell,L)}$ starts from a negative value at very low q^2 , rises rapidly toward positive values, and quickly becomes relatively flat. It has a maximum of ~ 0.9 in the mid q^2 region, followed by a slight decline at high q^2 . Similarly, the observable $P^{(\Xi_c^+,L)}$ for the longitudinally polarized daughter baryon in Fig. 11b starts negative and gradually increases towards the high q^2 region, after which it rapidly increases towards zero. It also has a large uncertainty deviation in the low q^2 region, which decreases towards the higher q^2 values. The crossing of the central and indicated uncertainty plots in Fig. 11b reminds us of the interference between the various terms in the amplitude involving the different form factors. Accordingly, as explained earlier, a more thorough analysis of form factor uncertainties is warranted with the uncertainty region only indicated by our analysis. Similar behaviors for both the central and uncertainty plots are also seen for the parent baryon in the longitudinal direction in Fig. 11c, except that the $P^{(\Xi_{cc}^{++},L)}$ is more or less constant and negative for the most part and only rapidly increases towards zero at the tail of the distribution for $q^2 \gtrsim 1.3\text{GeV}^2$.

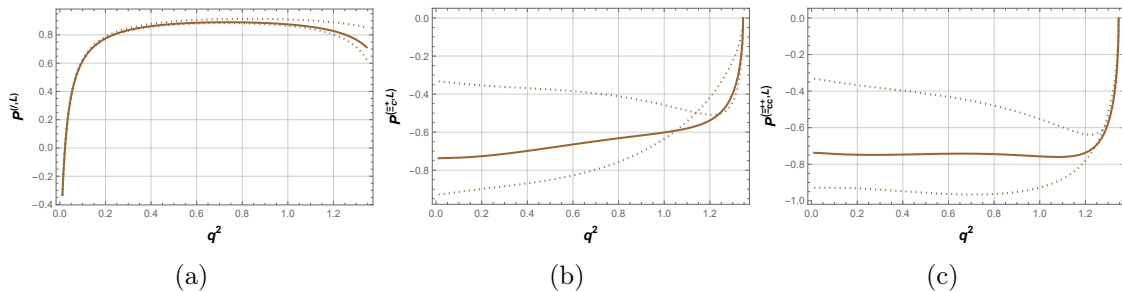


Figure 11. SM predictions for polarization asymmetries $P^{(m,n)}$ for particles m ($m \in \{\ell, \Xi_{cc}^{++}, \Xi_c^+\}$) in the longitudinal ($n = L$) direction.

In Fig. 12, we present the polarization asymmetries $P^{(m,T)}$ of the transversely polarized muon ℓ , daughter baryon Ξ_c^+ , and parent baryon Ξ_{cc}^{++} as a function of q^2 . For the muon ℓ , $P^{(\ell,T)}$ in Fig. 12a remains negative throughout the q^2 range, starting near -1 and gradually increasing towards zero at higher q^2 . Its uncertainty deviates slightly from the central plot in the mid-to-high q^2 region, after which this gap closes in at high q^2 . Furthermore, for

both the daughter and the parent baryons as shown in Figs. 12b and 12c, their respective observables $P^{(\Xi_c^+, T)}$ and $P^{(\Xi_{cc}^{++}, T)}$ start from zero. However, the former remains positive and monotonically increases throughout the dynamical q^2 range, whereas the latter is negative and monotonically decreases throughout the same range. Both their uncertainty plots deviate the most in the mid q^2 region, with this deviation only slightly decreasing in the high q^2 region.

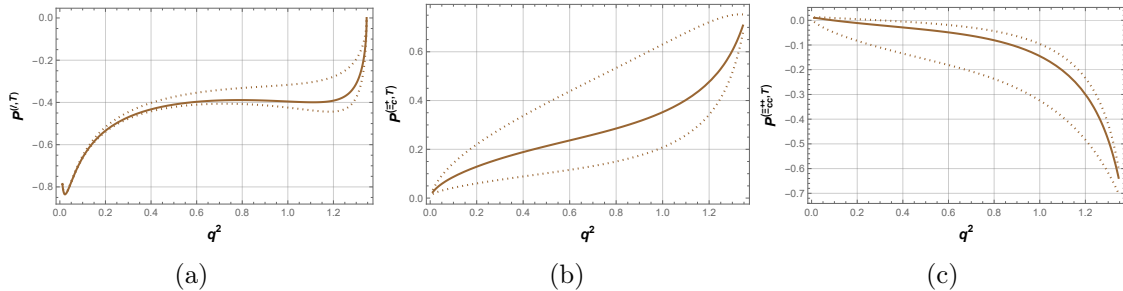


Figure 12. SM predictions for polarization asymmetries $P^{(m,n)}$ for particles m ($m \in \{\ell, \Xi_{cc}^{++}, \Xi_c^+\}$) in the transverse ($n = T$) direction.

We present the averaged values of the $P^{(m,L)}$ and $P^{(m,T)}$ over the q^2 bins: $[0.0112-0.4]$ GeV^2 , $[0.4-0.8]$ GeV^2 , $[0.8-0.1346]$ GeV^2 , and $[0.0112-0.1346]$ GeV^2 in Table 7 of Appendix A.

3.4.2 Polarization Ratios $\mathcal{R}_{nn'}^{(m,m')}[j]$

In order to further analyze the process, we now discuss the polarization ratios $\mathcal{R}_{nn'}^{(m,m')}[j]$. As described earlier, the ratio $\mathcal{R}_{nn'}^{(m,m')}[j]$ is a convenient measure for comparing the ‘numbers’ of m -type particles polarized with helicity j in the n direction with the m' -type particles polarized with helicity j in the n' direction.

We present the polarization ratios $\mathcal{R}_{nn'}^{(m,m')}[j]$ as a function of q^2 for different combinations of longitudinal and transverse polarizations in Figs. 13 and 14. Additionally, the results for various combinations of $\mathcal{R}_{nn'}^{(m,m')}[j]$ over the full dynamical q^2 range are provided in Table 8 of Appendix A.

In the ratios shown in Fig. 13, we observe that typically one helicity state has a larger value for the polarization ratio $\mathcal{R}_{nn'}^{(m,m')}[j]$. We can also see different combinations will have varying sensitivity to form factor uncertainties. Noticeably, in each ratio, one polarization case has more variation from their central plot than the other, where the latter is generated using the central values of the form factors. Figs. 13a, 13b, and 13c have significantly more such deviation in the negative (red) polarization state than in the positive (green) one, whereas Figs. 13d, 13e, 13f, 13g, and 13h more uncertainty is manifest in the positive (green) polarization state.

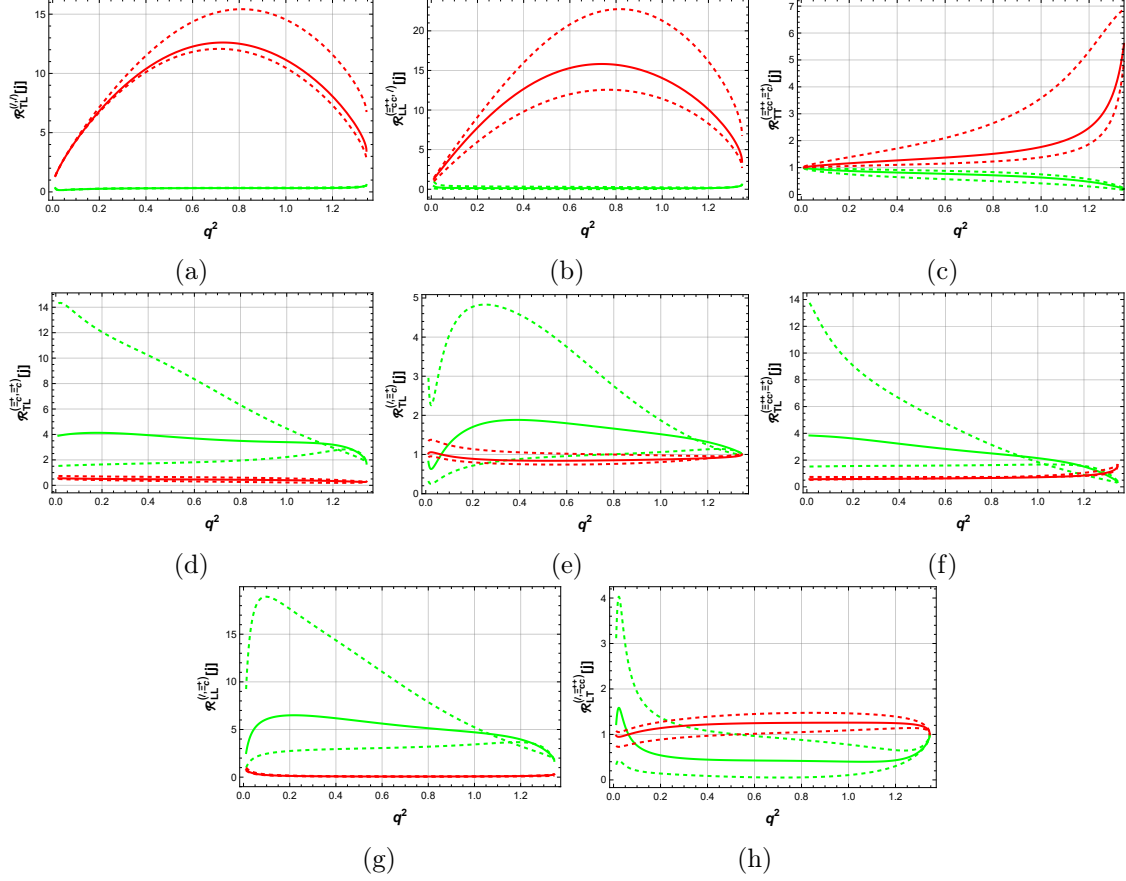


Figure 13. SM predictions for polarization ratios $\mathcal{R}_{nn'}^{(m,m')}[j]$ for different combinations of longitudinal and transverse polarizations as a function of q^2 , where there is a significant uncertainty in one of the polarization states.

The ratios in Fig. 14 highlight several “clean” observables, as both polarization cases have little deviation from the central plot. This suggests that polarization, which can be experimentally reconstructed from decay products in future experiments, may provide valuable insights into physics beyond the SM.

The variation in the magnitude of these ratios due to form factor uncertainties are shown in Fig. 15. Generally, we observe a smaller magnitude variation for most cases, except for the positively polarized cases of $\mathcal{R}_{TL}^{(\Xi_c^+, \Xi_c^+)}$, $\mathcal{R}_{TL}^{(\ell, \Xi_c^+)}$, $\mathcal{R}_{TL}^{(\Xi_{cc}^{++}, \Xi_c^+)}$, and $\mathcal{R}_{LL}^{(\ell, \Xi_c^+)}$ and the negative polarized cases of $\mathcal{R}_{TL}^{(\ell, \ell)}$ and $\mathcal{R}_{LL}^{(\Xi_{cc}^{++}, \ell)}$ where a larger variation is seen.

3.4.3 Polarization Asymmetry Ratios $\mathcal{R}_{P_{nn'}}^{(m,m')}$

We present the polarization asymmetry ratios $\mathcal{R}_{P_{nn'}}^{(m,m')}$ as a function of q^2 for some of the polarization ratios $\mathcal{R}_{nn'}^{(m,m')}$ found in the previous part in Fig. 16 as predicted by the SM. These indicate the differences in the positive ($k = +$) and negative ($k = -$) result of a particular polarization ratio. Their expressions are constructed in a way such that the deviations produced by the form factors uncertainties are minimized. The results are

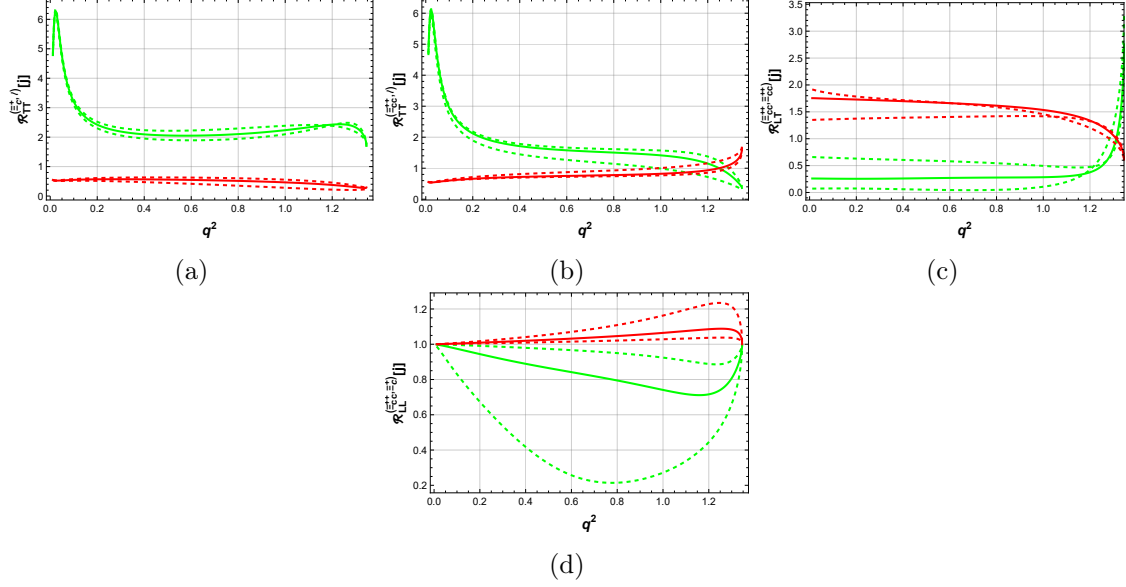


Figure 14. SM predictions for polarization ratios $\mathcal{R}_{nn'}^{(m,m')}[j]$ for different combinations of longitudinal and transverse polarizations as a function of q^2 , where there is minimal uncertainty for both polarization states.

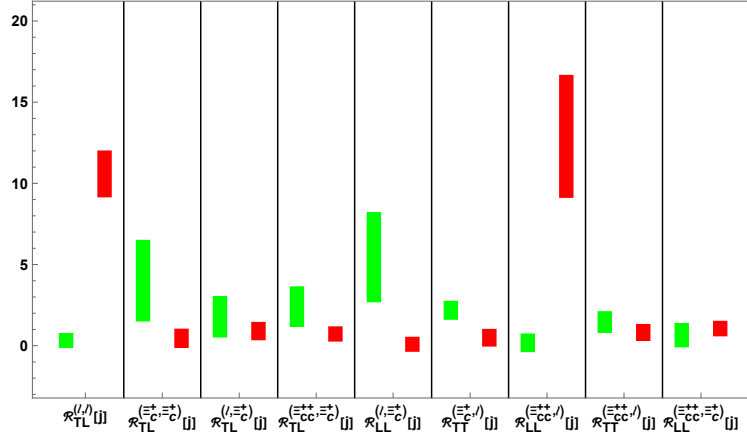


Figure 15. The variation in the magnitudes of the ratio $\mathcal{R}_{nn'}^{(m,m')}[j]$ for different polarization combinations of the particles m, m' ($m, m' \in \{\ell, \Xi_{cc}^{++}, \Xi_c^+\}$) in their respective direction n, n' ($n, n' \in \{L, T\}$) is shown. The index $j = \pm$ denotes the two polarization states, where the green bars correspond to $j = +$ and the red bars correspond to $j = -$.

also averaged over the q^2 bins: $[0.0112-0.4]$ GeV^2 , $[0.4-0.8]$ GeV^2 , $[0.8-0.1346]$ GeV^2 , and $[0.0112-0.1346]$ GeV^2 and their values along with related uncertainties are mentioned in Table 9 of Appendix A.

It can be evidently seen in all the plots in Fig. 16 that the uncertainty graphs do not deviate too much from their central plots. We can note that plots in Figs. 16b, 16c, 16d, and 16e differ somewhat more than the others in the low to mid q^2 range. This is because the plots of their corresponding polarization ratios - $\mathcal{R}_{TL}^{(\Xi_c^+, \Xi_c^+)}$, $\mathcal{R}_{TL}^{(\Xi_{cc}^{++}, \Xi_{cc}^{++})}$, $\mathcal{R}_{TL}^{(\ell, \Xi_c^+)}$,

and $\mathcal{R}_{TL}^{(\Xi_{cc}^{++}, \Xi_c^+)}$ - have a large variation between their respective uncertainty graphs for the positively polarized case in the low to mid q^2 range. Nevertheless, the relatively minimal uncertainty in these ratios throughout the q^2 range means that these ratios are good observables to test the SM and perhaps look for physics beyond the SM.

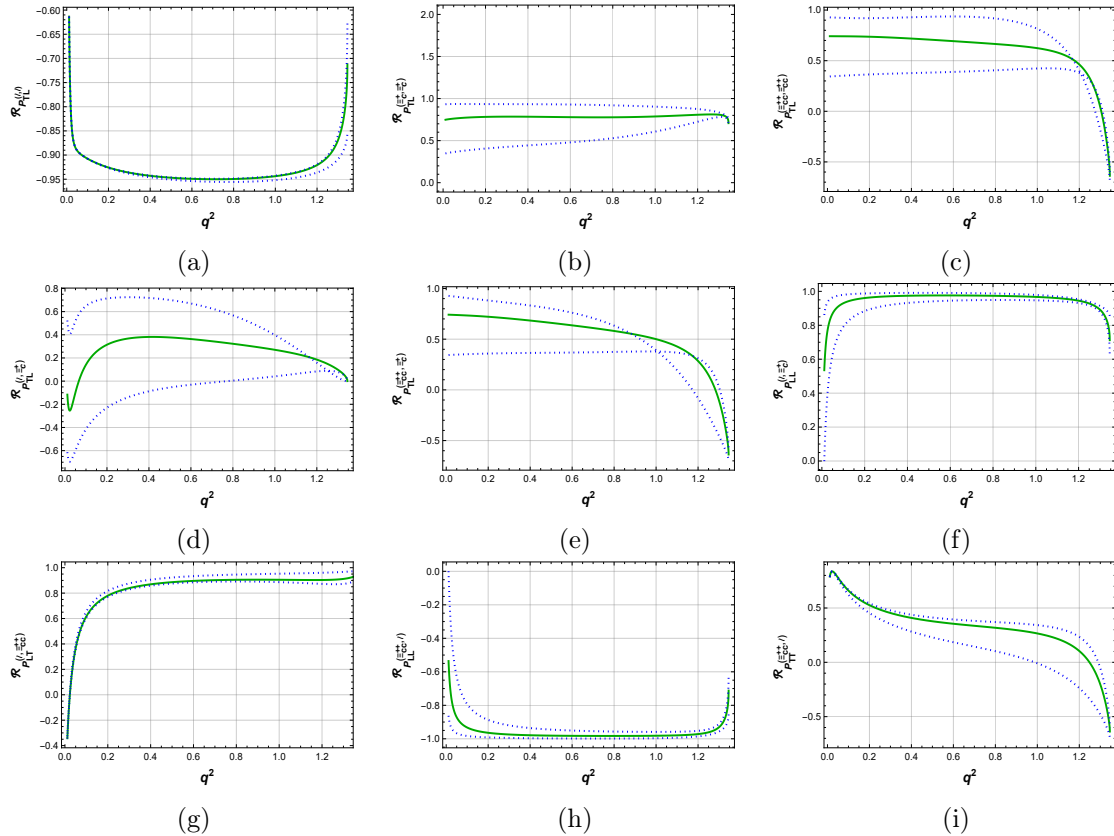


Figure 16. SM predictions for polarization asymmetries $\mathcal{R}_{P_{nn'}}^{(m, m')}$ for particles m, m' ($m, m' \in \{\ell, \Xi_{cc}^{++}, \Xi_c^+\}$) in the direction n, n' ($n, n' \in \{L, T\}$).

3.5 Correlation Analysis of Polarized Observables

Finally, we have computed the correlations between different observables of the $\Xi_{cc}^{++} \rightarrow \Xi_c^+ \bar{\mu} \nu_\mu$ decay, and have presented some representative plots in Fig. 17. The correlation plots between the differential branching ratio and the forward-backward asymmetry for the positively polarized particles show that the magnitude of the latter decreases as the former increases. The differences between the longitudinal and transverse polarization configurations show the sensitivities to the helicity structure of the weak interaction. The correlations among different differential branching ratios are nearly linear across the physical parameter space. Such linear trends indicate that the underlying helicity amplitudes contributing to different polarization channels are strongly correlated. The separation between the $k = +$ and $k = -$ polarization states in these plots further highlights the sensitivity of polarized observables. These correlations provide valuable complementary information for testing the SM and probing possible NP effects.

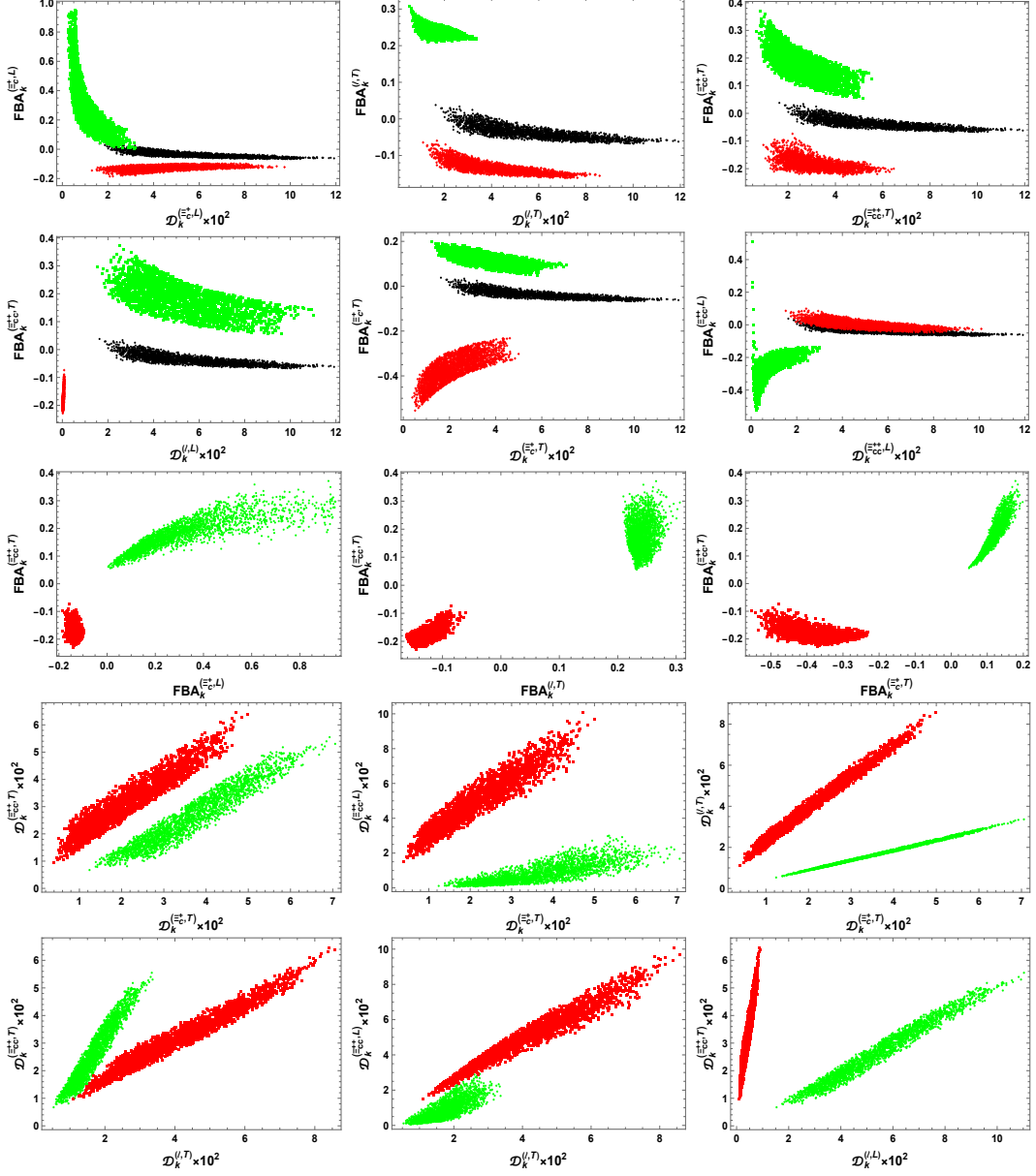


Figure 17. Correlations between $FBA_k^{(m,n)}$ and $\mathcal{D}_k^{(m',n')}$, between $FBA_k^{(m,n)}$ and $FBA_k^{(m',n')}$, and between $\mathcal{D}_k^{(m,n)}$ and $\mathcal{D}_k^{(m',n')}$ for particles m, m' ($m, m' \in \{\ell, \Xi_{cc}^{++}, \Xi_c^+\}$) in their respective polarization direction n, n' ($n, n' \in \{L, T\}$). The black, green, and red points indicate unpolarized, positive polarization, and negative polarization cases, respectively.

4 Summary and Conclusion

In this work, we have studied the semileptonic decay $\Xi_{cc}^{++} \rightarrow \Xi_c^+ \bar{\ell} \nu_\ell$, which proceeds through the quark-level transition $c \rightarrow s$. This decay channel provides an important framework for probing the dynamics of heavy baryons and for testing the structure of weak interactions in the baryon sector. In particular, we investigated the role of polarization of particles associated with this decay on various physical observables.

Using the form factors obtained from QCD sum rules, we calculated the q^2 -dependent observables, which include the differential branching ratio $\mathcal{D}(q^2)$ and the forward-backward asymmetry $\text{FBA}(q^2)$. We analyzed these observables for different particle polarization configurations, with both longitudinal and transverse polarization states being considered. Our analysis shows that polarization effects can significantly modify the behavior of branching ratios and forward-backward asymmetries across the full q^2 range. These polarized observables exhibit distinct patterns and hierarchies for different spin configurations. We also evaluated the spin polarization asymmetries $P^{(m,n)}$ of the muon and baryons, which further illustrate the sensitivity of the decay observables to the polarization states of the participating particles. Furthermore, we defined and computed polarization asymmetry ratios for different combinations of longitudinal and transverse polarization states. These ratios exhibit noticeable variations depending on the polarization configuration, indicating that polarization observables, especially polarization asymmetry ratios, may provide additional sensitive probes in future experimental studies. In addition, we computed the LFU ratio and by integrating over the full q^2 range, we obtained $\mathcal{R}_{\Xi_c^+}(\mu/e) = 1.00229_{-0.01551}^{+0.00374}$.

Finally, we also examined correlations among different observables of the decay $\Xi_{cc}^{++} \rightarrow \Xi_c^+ \ell^+ \nu_\ell$, including cases with different polarization states of the involved particles. Such correlations may help in identifying clean observables that can be used to test the SM predictions more precisely.

Overall, our results demonstrate that polarization effects play a significant role in the phenomenology of the decay $\Xi_{cc}^{++} \rightarrow \Xi_c^+ \bar{\ell} \nu_\ell$. The study of polarized observables and ratios in this channel may serve as a useful probe for future experimental measurements and possible physics effects beyond the SM.

Appendix

A Tables of Numerical Results

$\tilde{\mathcal{D}} \times 10^2$	$\tilde{\mathcal{D}}_+^{(\ell,L)} \times 10^2$	$\tilde{\mathcal{D}}_+^{(\Xi_c^+,L)} \times 10^2$	$\tilde{\mathcal{D}}_+^{(\Xi_{cc}^{++},L)} \times 10^2$	$\tilde{\mathcal{D}}_+^{(\ell,T)} \times 10^2$	$\tilde{\mathcal{D}}_+^{(\Xi_c^+,T)} \times 10^2$	$\tilde{\mathcal{D}}_+^{(\Xi_{cc}^{++},T)} \times 10^2$
$5.52_{-3.35}^{+6.32}$	$5.13_{-3.09}^{+5.82}$	$0.98_{-0.72}^{+2.54}$	$0.79_{-0.71}^{+2.57}$	$1.61_{-0.92}^{+1.73}$	$3.51_{-1.91}^{+3.30}$	$2.51_{-1.67}^{+3.10}$
$\tilde{\mathcal{D}} \times 10^2$	$\tilde{\mathcal{D}}_-^{(\ell,L)} \times 10^2$	$\tilde{\mathcal{D}}_-^{(\Xi_c^+,L)} \times 10^2$	$\tilde{\mathcal{D}}_-^{(\Xi_{cc}^{++},L)} \times 10^2$	$\tilde{\mathcal{D}}_-^{(\ell,T)} \times 10^2$	$\tilde{\mathcal{D}}_-^{(\Xi_c^+,T)} \times 10^2$	$\tilde{\mathcal{D}}_-^{(\Xi_{cc}^{++},T)} \times 10^2$
$5.52_{-3.35}^{+6.32}$	$0.39_{-0.26}^{+0.50}$	$4.54_{-2.64}^{+3.78}$	$4.73_{-2.65}^{+3.75}$	$3.91_{-2.43}^{+4.60}$	$2.02_{-1.44}^{+3.02}$	$3.01_{-1.68}^{+3.22}$
FBA	$\text{FBA}_+^{(\ell,L)}$	$\text{FBA}_+^{(\Xi_c^+,L)}$	$\text{FBA}_+^{(\Xi_{cc}^{++},L)}$	$\text{FBA}_+^{(\ell,T)}$	$\text{FBA}_+^{(\Xi_c^+,T)}$	$\text{FBA}_+^{(\Xi_{cc}^{++},T)}$
$-0.045_{-0.014}^{+0.027}$	$0.021_{-0.013}^{+0.028}$	$0.165_{-0.155}^{+0.399}$	$-0.195_{-0.164}^{+0.062}$	$0.191_{-0.014}^{+0.037}$	$0.074_{-0.019}^{+0.013}$	$0.069_{-0.046}^{-0.012}$
FBA	$\text{FBA}_-^{(\ell,L)}$	$\text{FBA}_-^{(\Xi_c^+,L)}$	$\text{FBA}_-^{(\Xi_{cc}^{++},L)}$	$\text{FBA}_-^{(\ell,T)}$	$\text{FBA}_-^{(\Xi_c^+,T)}$	$\text{FBA}_-^{(\Xi_{cc}^{++},T)}$
$-0.045_{-0.014}^{+0.027}$	$-0.631_{-0.041}^{+0.005}$	$-0.087_{-0.001}^{+0.002}$	$-0.020_{-0.007}^{+0.017}$	$-0.131_{-0.010}^{+0.014}$	$-0.235_{-0.023}^{+0.030}$	$-0.144_{-0.022}^{+0.097}$

Table 3. Ranges of branching ratios and forward-backward asymmetry for $q^2 = [0.0112 - 1.346]$ GeV^2 .

$\tilde{\mathcal{D}} \times 10^2$	$\tilde{\mathcal{D}}_+^{(\ell,L)} \times 10^2$	$\tilde{\mathcal{D}}_+^{(\Xi_c^+,L)} \times 10^2$	$\tilde{\mathcal{D}}_+^{(\Xi_{cc}^{++},L)} \times 10^2$	$\tilde{\mathcal{D}}_+^{(\ell,T)} \times 10^2$	$\tilde{\mathcal{D}}_+^{(\Xi_c^+,T)} \times 10^2$	$\tilde{\mathcal{D}}_+^{(\Xi_{cc}^{++},T)} \times 10^2$
$2.78_{-1.58}^{+3.27}$	$2.49_{-1.41}^{+2.92}$	$0.39_{-0.33}^{+1.55}$	$0.36_{-0.33}^{+1.55}$	$0.68_{-0.38}^{+0.79}$	$1.59_{-0.84}^{+1.64}$	$1.37_{-0.83}^{+1.66}$
$\tilde{\mathcal{D}} \times 10^2$	$\tilde{\mathcal{D}}_-^{(\ell,L)} \times 10^2$	$\tilde{\mathcal{D}}_-^{(\Xi_c^+,L)} \times 10^2$	$\tilde{\mathcal{D}}_-^{(\Xi_{cc}^{++},L)} \times 10^2$	$\tilde{\mathcal{D}}_-^{(\ell,T)} \times 10^2$	$\tilde{\mathcal{D}}_-^{(\Xi_c^+,T)} \times 10^2$	$\tilde{\mathcal{D}}_-^{(\Xi_{cc}^{++},T)} \times 10^2$
$2.78_{-1.58}^{+3.27}$	$0.29_{-0.17}^{+0.36}$	$2.39_{-1.26}^{+1.73}$	$2.42_{-1.26}^{+1.72}$	$2.09_{-1.21}^{+2.49}$	$1.18_{-0.74}^{+1.63}$	$1.41_{-0.76}^{+1.61}$
FBA	$\text{FBA}_+^{(\ell,L)}$	$\text{FBA}_+^{(\Xi_c^+,L)}$	$\text{FBA}_+^{(\Xi_{cc}^{++},L)}$	$\text{FBA}_+^{(\ell,T)}$	$\text{FBA}_+^{(\Xi_c^+,T)}$	$\text{FBA}_+^{(\Xi_{cc}^{++},T)}$
$-0.282_{-0.011}^{+0.020}$	$0.017_{-0.011}^{+0.020}$	$-0.152_{-0.119}^{+0.658}$	$-0.357_{+0.026}^{+0.045}$	$0.690_{-0.014}^{+0.030}$	$-0.101_{-0.039}^{+0.035}$	$-0.157_{-0.115}^{+0.001}$
FBA	$\text{FBA}_-^{(\ell,L)}$	$\text{FBA}_-^{(\Xi_c^+,L)}$	$\text{FBA}_-^{(\Xi_{cc}^{++},L)}$	$\text{FBA}_-^{(\ell,T)}$	$\text{FBA}_-^{(\Xi_c^+,T)}$	$\text{FBA}_-^{(\Xi_{cc}^{++},T)}$
$-0.282_{-0.011}^{+0.020}$	$-1.861_{-0.026}^{+0.005}$	$-0.3023_{-0.0009}^{+0.0002}$	$-0.270_{-0.004}^{+0.010}$	$-0.544_{-0.007}^{+0.006}$	$-0.512_{-0.048}^{+0.048}$	$-0.404_{-0.027}^{+0.151}$

Table 4. Ranges of branching ratios and forward-backward asymmetry for $q^2 = [0.0112 - 0.4]$ GeV^2 .

$\tilde{\mathcal{D}} \times 10^2$	$\tilde{\mathcal{D}}_+^{(\ell,L)} \times 10^2$	$\tilde{\mathcal{D}}_+^{(\Xi_c^+,L)} \times 10^2$	$\tilde{\mathcal{D}}_+^{(\Xi_{cc}^{++},L)} \times 10^2$	$\tilde{\mathcal{D}}_+^{(\ell,T)} \times 10^2$	$\tilde{\mathcal{D}}_+^{(\Xi_c^+,T)} \times 10^2$	$\tilde{\mathcal{D}}_+^{(\Xi_{cc}^{++},T)} \times 10^2$
$5.89_{-3.58}^{+6.90}$	$5.55_{-3.35}^{+6.46}$	$0.99_{-0.79}^{+2.93}$	$0.83_{-0.78}^{+2.96}$	$1.77_{-1.02}^{+1.98}$	$3.65_{-1.99}^{+3.50}$	$2.80_{-1.85}^{+3.47}$
$\tilde{\mathcal{D}} \times 10^2$	$\tilde{\mathcal{D}}_-^{(\ell,L)} \times 10^2$	$\tilde{\mathcal{D}}_-^{(\Xi_c^+,L)} \times 10^2$	$\tilde{\mathcal{D}}_-^{(\Xi_{cc}^{++},L)} \times 10^2$	$\tilde{\mathcal{D}}_-^{(\ell,T)} \times 10^2$	$\tilde{\mathcal{D}}_-^{(\Xi_c^+,T)} \times 10^2$	$\tilde{\mathcal{D}}_-^{(\Xi_{cc}^{++},T)} \times 10^2$
$5.89_{-3.58}^{+6.90}$	$0.34_{-0.23}^{+0.44}$	$4.90_{-2.80}^{+3.97}$	$5.06_{-2.80}^{+3.94}$	$4.13_{-2.56}^{+4.92}$	$2.25_{-1.60}^{+3.40}$	$3.10_{-1.73}^{+3.43}$
FBA	$\text{FBA}_+^{(\ell,L)}$	$\text{FBA}_+^{(\Xi_c^+,L)}$	$\text{FBA}_+^{(\Xi_{cc}^{++},L)}$	$\text{FBA}_+^{(\ell,T)}$	$\text{FBA}_+^{(\Xi_c^+,T)}$	$\text{FBA}_+^{(\Xi_{cc}^{++},T)}$
$-0.040_{-0.033}^{+0.079}$	$0.052_{-0.032}^{+0.072}$	$0.351_{-0.302}^{+1.175}$	$-0.297_{-0.286}^{+0.097}$	$0.437_{-0.037}^{+0.082}$	$0.266_{-0.043}^{+0.043}$	$0.264_{-0.116}^{+0.029}$
FBA	$\text{FBA}_-^{(\ell,L)}$	$\text{FBA}_-^{(\Xi_c^+,L)}$	$\text{FBA}_-^{(\Xi_{cc}^{++},L)}$	$\text{FBA}_-^{(\ell,T)}$	$\text{FBA}_-^{(\Xi_c^+,T)}$	$\text{FBA}_-^{(\Xi_{cc}^{++},T)}$
$-0.040_{-0.033}^{+0.079}$	$-1.504_{-0.088}^{+0.010}$	$-0.118_{-0.009}^{+0.015}$	$0.003_{-0.022}^{+0.052}$	$-0.243_{-0.026}^{+0.057}$	$-0.533_{-0.108}^{+0.087}$	$-0.315_{-0.055}^{+0.278}$

Table 5. Ranges of branching ratios and forward-backward asymmetry for $q^2 = [0.4 - 0.8]$ GeV^2 .

$\tilde{\mathcal{D}} \times 10^2$	$\tilde{\mathcal{D}}_+^{(\ell,L)} \times 10^2$	$\tilde{\mathcal{D}}_+^{(\Xi_c^+,L)} \times 10^2$	$\tilde{\mathcal{D}}_+^{(\Xi_{cc}^{++},L)} \times 10^2$	$\tilde{\mathcal{D}}_+^{(\ell,T)} \times 10^2$	$\tilde{\mathcal{D}}_+^{(\Xi_c^+,T)} \times 10^2$	$\tilde{\mathcal{D}}_+^{(\Xi_{cc}^{++},T)} \times 10^2$
$3.82_{-2.39}^{+4.19}$	$3.56_{-2.20}^{+3.86}$	$0.79_{-0.50}^{+1.40}$	$0.59_{-0.49}^{+1.43}$	$1.17_{-0.67}^{+1.15}$	$2.61_{-1.45}^{+2.31}$	$1.58_{-1.12}^{+1.95}$
$\tilde{\mathcal{D}} \times 10^2$	$\tilde{\mathcal{D}}_-^{(\ell,L)} \times 10^2$	$\tilde{\mathcal{D}}_-^{(\Xi_c^+,L)} \times 10^2$	$\tilde{\mathcal{D}}_-^{(\Xi_{cc}^{++},L)} \times 10^2$	$\tilde{\mathcal{D}}_-^{(\ell,T)} \times 10^2$	$\tilde{\mathcal{D}}_-^{(\Xi_c^+,T)} \times 10^2$	$\tilde{\mathcal{D}}_-^{(\Xi_{cc}^{++},T)} \times 10^2$
$3.82_{-2.39}^{+4.19}$	$0.26_{-0.19}^{+0.33}$	$3.03_{-1.89}^{+2.79}$	$3.23_{-1.90}^{+2.76}$	$2.65_{-1.72}^{+3.04}$	$1.20_{-0.94}^{+1.89}$	$2.24_{-1.28}^{+2.25}$
FBA	$\text{FBA}_+^{(\ell,L)}$	$\text{FBA}_+^{(\Xi_c^+,L)}$	$\text{FBA}_+^{(\Xi_{cc}^{++},L)}$	$\text{FBA}_+^{(\ell,T)}$	$\text{FBA}_+^{(\Xi_c^+,T)}$	$\text{FBA}_+^{(\Xi_{cc}^{++},T)}$
$0.025_{-0.047}^{+0.119}$	$0.076_{-0.045}^{+0.111}$	$0.733_{-0.359}^{+0.522}$	$-0.628_{-0.405}^{+0.218}$	$0.246_{-0.049}^{+0.116}$	$0.314_{-0.026}^{+0.026}$	$0.457_{-0.064}^{+0.053}$
FBA	$\text{FBA}_-^{(\ell,L)}$	$\text{FBA}_-^{(\Xi_c^+,L)}$	$\text{FBA}_-^{(\Xi_{cc}^{++},L)}$	$\text{FBA}_-^{(\ell,T)}$	$\text{FBA}_-^{(\Xi_c^+,T)}$	$\text{FBA}_-^{(\Xi_{cc}^{++},T)}$
$0.025_{-0.047}^{+0.119}$	$-0.654_{-0.057}^{+0.002}$	$-0.167_{-0.004}^{+0.008}$	$0.150_{-0.042}^{+0.101}$	$-0.074_{-0.038}^{+0.099}$	$-0.631_{-0.128}^{+0.337}$	$-0.267_{-0.069}^{+0.242}$

Table 6. Ranges of branching ratios and forward-backward asymmetry for $q^2 = [0.8 - 1.346]$ GeV^2 .

Observables	$[0.0112 - 0.4]$ GeV^2	$[0.4 - 0.8]$ GeV^2	$[0.8 - 1.346]$ GeV^2	$[0.0112 - 1.346]$ GeV^2
$P^{(\ell,L)}$	(1.744,1.772)	(2.192,2.254)	(1.546,1.653)	(0.788,0.811)
$P^{(\Xi_c^+,L)}$	(-2.314,-0.907)	(-2.065,-0.964)	(-1.048,-0.832)	(-0.793,-0.390)
$P^{(\Xi_{cc}^{++},L)}$	(-2.401,-0.922)	(-2.381,-1.015)	(-1.526,-0.909)	(-0.914,-0.411)
$P^{(\ell,T)}$	(-1.492,-1.444)	(-1.040,-0.900)	(-0.767,-0.546)	(-0.430,-0.483)
$P^{(\Xi_c^+,T)}$	(0.149,0.533)	(0.289,1.079)	(0.454,1.177)	(0.127,0.389)
$P^{(\Xi_{cc}^{++},T)}$	(-0.201,0.012)	(-0.449,-0.050)	(-0.678,-0.255)	(-0.185,-0.042)

Table 7. Ranges of polarization asymmetries in different q^2 bins.

$\mathcal{R}_{TL}^{(\ell,\ell)}[+]$	$\mathcal{R}_{TL}^{(\ell,\ell)}[-]$	$\mathcal{R}_{TL}^{(\Xi_c^+, \Xi_c^+)}[+]$	$\mathcal{R}_{TL}^{(\Xi_c^+, \Xi_c^+)}[-]$	$\mathcal{R}_{TL}^{(\ell, \Xi_c^+)}[+]$	$\mathcal{R}_{TL}^{(\ell, \Xi_c^+)}[-]$
(0.304, 0.336)	(9.58, 11.6)	(1.94, 6.08)	(0.302, 0.605)	(0.948, 2.62)	(0.778, 1.02)
$\mathcal{R}_{TL}^{(\Xi_{cc}^{++}, \Xi_c^+)}[+]$	$\mathcal{R}_{TL}^{(\Xi_{cc}^{++}, \Xi_c^+)}[-]$	$\mathcal{R}_{LL}^{(\ell, \Xi_c^+)}[+]$	$\mathcal{R}_{LL}^{(\ell, \Xi_c^+)}[-]$	$\mathcal{R}_{TT}^{(\Xi_c^+, \ell)}[+]$	$\mathcal{R}_{TT}^{(\Xi_c^+, \ell)}[-]$
(1.60, 3.21)	(0.696, 0.749)	(3.12, 7.79)	(0.107, 0.067)	(2.04, 2.32)	(0.389, 0.592)
$\mathcal{R}_{LL}^{(\Xi_{cc}^{++}, \ell)}[+]$	$\mathcal{R}_{LL}^{(\Xi_{cc}^{++}, \ell)}[-]$	$\mathcal{R}_{TT}^{(\Xi_{cc}^{++}, \ell)}[+]$	$\mathcal{R}_{TT}^{(\Xi_{cc}^{++}, \ell)}[-]$	$\mathcal{R}_{LL}^{(\Xi_{cc}^{++}, \Xi_c^+)}[+]$	$\mathcal{R}_{LL}^{(\Xi_{cc}^{++}, \Xi_c^+)}[-]$
(0.044, 0.307)	(9.55, 16.2)	(1.23, 1.68)	(0.733, 0.895)	(0.343, 0.956)	(1.02, 1.09)

Table 8. Ranges of the polarization ratios for different polarization combinations of the muon ℓ , Ξ_c^+ , and Ξ_{cc}^{++} .

Observables	[0.0112 – 0.4] GeV ²	[0.4 – 0.8] GeV ²	[0.8 – 1.346] GeV ²	[0.0112 – 1.346] GeV ²
$\mathcal{R}_{P_{TL}^{(\ell,\ell)}}$	(-2.384, -2.381)	(-2.382, -2.369)	(-1.738, -1.718)	(-0.944, -0.938)
$\mathcal{R}_{P_{TL}^{(\Xi_c^+, \Xi_c^+)}}$	(1.073, 2.400)	(1.207, 2.317)	(1.134, 1.639)	(0.524, 0.905)
$\mathcal{R}_{P_{TL}^{(\Xi_{cc}^{++}, \Xi_{cc}^{++})}}$	(0.947, 2.374)	(0.975, 2.331)	(0.734, 1.351)	(0.388, 0.872)
$\mathcal{R}_{P_{TL}^{(\ell, \Xi_c^+)}}$	(-0.489, 1.828)	(-0.082, 1.645)	(0.075, 0.668)	(-0.037, 0.542)
$\mathcal{R}_{P_{LT}^{(\ell, \Xi_{cc}^{++})}}$	(2.019, 2.145)	(2.206, 2.330)	(1.616, 1.746)	(0.864, 0.923)
$\mathcal{R}_{P_{TL}^{(\Xi_{cc}^{++}, \Xi_c^+)}}$	(0.926, 2.231)	(0.922, 1.881)	(0.595, 0.650)	(0.361, 0.644)
$\mathcal{R}_{P_{LL}^{(\ell, \Xi_c^+)}}$	(2.296, 2.539)	(2.360, 2.475)	(1.726, 1.788)	(0.934, 0.983)
$\mathcal{R}_{P_{LL}^{(\Xi_{cc}^{++}, \ell)}}$	(-2.553, -2.301)	(-2.494, -2.367)	(-1.819, -1.737)	(-0.995, -0.938)
$\mathcal{R}_{P_{TT}^{(\Xi_{cc}^{++}, \ell)}}$	(1.050, 1.324)	(0.467, 0.992)	(-0.082, 0.584)	(0.156, 0.393)

Table 9. Ranges of the polarization asymmetry ratios in different q^2 bins for different polarization combinations of the muon ℓ , Ξ_c^+ , and Ξ_{cc}^{++} .

B Decay Amplitudes for Polarized Particles

$$\begin{aligned}
|\mathcal{A}_k^{(\ell, L)}|^2 &= \frac{4}{3q^4} (q^2 - m_\mu^2) \left\{ 2 \left\{ 12q^4(k+1)M_{\Xi_c^+}M_{\Xi_{cc}^{++}}[-\mathcal{F}_1^2 + \mathcal{G}_1^2] + (k-1)m_\mu^2 \right. \right. \\
&\quad \times \left[2(\mathcal{F}_1^2 + \mathcal{G}_1^2) + \frac{1}{M_{\Xi_c^+}M_{\Xi_{cc}^{++}}} [Q_+\mathcal{F}_2\mathcal{F}_3 + Q_-\mathcal{G}_2\mathcal{G}_3] \right] \left[q^4 + q^2(M_{\Xi_c^+}^2 + M_{\Xi_{cc}^{++}}^2) \right. \\
&\quad \left. \left. - 2(M_{\Xi_c^+}^2 - M_{\Xi_{cc}^{++}}^2)^2 \right] - 2q^2(k+1)(\mathcal{F}_1^2 + \mathcal{G}_1^2) [2q^4 - q^2(M_{\Xi_c^+}^2 + M_{\Xi_{cc}^{++}}^2) \right. \\
&\quad \left. \left. - (M_{\Xi_c^+}^2 - M_{\Xi_{cc}^{++}}^2)^2 \right] \right\} + \left\{ Q_+Q_-q^2(k+1) \left[\frac{Q_+\mathcal{F}_2}{M_{\Xi_{cc}^{++}}} \left(\frac{\mathcal{F}_2}{M_{\Xi_{cc}^{++}}} + \frac{\mathcal{F}_3}{M_{\Xi_c^+}} \right) \right. \right. \\
&\quad \left. \left. + \frac{Q_-\mathcal{G}_2}{M_{\Xi_{cc}^{++}}} \left(\frac{\mathcal{G}_2}{M_{\Xi_{cc}^{++}}} + \frac{\mathcal{G}_3}{M_{\Xi_c^+}} \right) \right] \right\} + \left\{ -2(k-1)m_\mu^2\Omega \left[Q_+ \left(\frac{\mathcal{F}_2^2}{M_{\Xi_{cc}^{++}}^2} + \frac{\mathcal{F}_3^2}{M_{\Xi_c^+}^2} \right) \right. \right. \\
&\quad \left. \left. + Q_- \left(\frac{\mathcal{G}_2^2}{M_{\Xi_{cc}^{++}}^2} + \frac{\mathcal{G}_3^2}{M_{\Xi_c^+}^2} \right) \right] + \frac{2}{M_{\Xi_{cc}^{++}}^2} q^2(k-1)m_\mu^2 [Q_+\mathcal{F}_2^2 + Q_-\mathcal{G}_2^2] \right\}
\end{aligned}$$

$$\begin{aligned}
& \times (2M_{\Xi_c^+}^2 - M_{\Xi_{cc}^{++}}^2) + \frac{1}{M_{\Xi_c^+}^2} [Q_+ \mathcal{F}_3^2 + Q_- \mathcal{G}_3^2] [2(k-1)(M_{\Xi_c^+}^2 + 2M_{\Xi_{cc}^{++}}^2) \\
& - q^2(k+1)][(M_{\Xi_c^+}^2 - M_{\Xi_{cc}^{++}}^2) + q^2] \Big\} + 4 \left\{ -2(k-1)m_\mu^2 \left[\left[Q_+ \mathcal{F}_1 \left(\frac{\mathcal{F}_2}{M_{\Xi_{cc}^{++}} + M_{\Xi_c^+}} + \frac{\mathcal{F}_3}{M_{\Xi_c^+}} \right) \right] \right. \right. \\
& + \left. \left[Q_- \mathcal{G}_1 \left(\frac{\mathcal{G}_2}{M_{\Xi_{cc}^{++}} + M_{\Xi_c^+}} + \frac{\mathcal{G}_3}{M_{\Xi_c^+}} \right) \right] \right] (M_{\Xi_c^+} + M_{\Xi_{cc}^{++}})(M_{\Xi_c^+} - M_{\Xi_{cc}^{++}})^2 + Q_+ Q_- q^2(k+1) \\
& \times (M_{\Xi_c^+} + M_{\Xi_{cc}^{++}}) \left[\left[\mathcal{F}_1 \left(\frac{\mathcal{F}_2}{M_{\Xi_{cc}^{++}} + M_{\Xi_c^+}} + \frac{\mathcal{F}_3}{M_{\Xi_c^+}} \right) \right] + \left[\mathcal{G}_1 \left(\frac{\mathcal{G}_2}{M_{\Xi_{cc}^{++}} + M_{\Xi_c^+}} + \frac{\mathcal{G}_3}{M_{\Xi_c^+}} \right) \right] \right] \\
& + q^2(k-1)m_\mu^2 \left[Q_+ \mathcal{F}_1 \left(\frac{\mathcal{F}_2}{M_{\Xi_{cc}^{++}} + M_{\Xi_c^+}} (2M_{\Xi_c^+} - M_{\Xi_{cc}^{++}}) - \frac{\mathcal{F}_3}{M_{\Xi_c^+}} (M_{\Xi_c^+} - 2M_{\Xi_{cc}^{++}}) \right) \right. \\
& \left. + Q_- \mathcal{G}_1 \left(\frac{\mathcal{G}_2}{M_{\Xi_{cc}^{++}} + M_{\Xi_c^+}} (2M_{\Xi_c^+} + M_{\Xi_{cc}^{++}}) - \frac{\mathcal{G}_3}{M_{\Xi_c^+}} (M_{\Xi_c^+} + 2M_{\Xi_{cc}^{++}}) \right) \right] \Big\}, \tag{B.1}
\end{aligned}$$

where $\Omega \equiv [(M_{\Xi_c^+}^2 - M_{\Xi_{cc}^{++}}^2)^2 - q^4]$.

$$\begin{aligned}
|\mathcal{A}_k^{(\Xi_c^+, L)}|^2 &= \frac{-2}{3q^4} (q^2 - m_\mu^2) \left\{ 4\Omega [\mathcal{F}_1^2 + \mathcal{G}_1^2] [3m_\mu^2(k-1) - q^2(k+1)] + \lambda [m_\mu^2(k-1) \right. \\
& + q^2(k+1)] + 48q^4 M_{\Xi_c^+} M_{\Xi_{cc}^{++}} (k+1) [\mathcal{F}_1^2 - \mathcal{G}_1^2] + 4(M_{\Xi_c^+} + M_{\Xi_{cc}^{++}}) \\
& \times [m_\mu^2 \lambda (k-1) - Q_+ q^2(k+1) - \lambda] \mathcal{F}_1 \left[\frac{\mathcal{F}_2}{M_{\Xi_{cc}^{++}} + M_{\Xi_c^+}} + \frac{\mathcal{F}_3}{M_{\Xi_c^+}} \right] + 4Q_+ m_\mu^2 (k-1) \\
& \times (M_{\Xi_c^+} - M_{\Xi_{cc}^{++}}) \mathcal{F}_1 \left[\frac{\mathcal{F}_2}{M_{\Xi_{cc}^{++}} + M_{\Xi_c^+}} (M_{\Xi_c^+}^2 - M_{\Xi_{cc}^{++}}^2 - q^2) + \frac{\mathcal{F}_3}{M_{\Xi_c^+}} (M_{\Xi_c^+}^2 - M_{\Xi_{cc}^{++}}^2 + q^2) \right] \\
& + m_\mu^2 (k-1) \left[\frac{1}{M_{\Xi_{cc}^{++}}^2} [Q_+ \mathcal{F}_2^2 + Q_- \mathcal{G}_2^2] [\lambda + 3(M_{\Xi_c^+} M_{\Xi_{cc}^{++}} - q^2)^2] \right. \\
& + \frac{2}{M_{\Xi_c^+} M_{\Xi_{cc}^{++}}} [Q_+ \mathcal{F}_2 \mathcal{F}_3 + Q_- \mathcal{G}_2 \mathcal{G}_3] [3\Omega + \lambda] + \frac{1}{M_{\Xi_c^+}^2} [Q_+ \mathcal{F}_3^2 + Q_- \mathcal{G}_3^2] \\
& \times [3\tilde{\Omega} + \lambda] \Big] - q^2(k+1)(3Q_+ Q_- - \lambda) \left[Q_+ \left(\frac{\mathcal{F}_2^2}{M_{\Xi_{cc}^{++}}^2} + \frac{\mathcal{F}_3^2}{M_{\Xi_c^+}^2} \right)^2 \right. \\
& + Q_- \left(\frac{\mathcal{G}_2^2}{M_{\Xi_{cc}^{++}}^2} + \frac{\mathcal{G}_3^2}{M_{\Xi_c^+}^2} \right)^2 - 8q^2 (M_{\Xi_c^+} - M_{\Xi_{cc}^{++}}) \mathcal{G}_1 \left(\frac{\mathcal{G}_2^2}{M_{\Xi_{cc}^{++}}^2} + \frac{\mathcal{G}_3^2}{M_{\Xi_c^+}^2} \right) \\
& + 4m_\mu^2 \mathcal{G}_1 \left[[m_\mu^2 (k-1)(M_{\Xi_c^+} - M_{\Xi_{cc}^{++}}) [3Q_- (M_{\Xi_c^+} + M_{\Xi_{cc}^{++}})^2 + \lambda]] \right. \\
& - 2q^2 [3kQ_- (M_{\Xi_c^+} + M_{\Xi_{cc}^{++}})^2 - \lambda] \left[\frac{\mathcal{G}_2}{M_{\Xi_{cc}^{++}} + M_{\Xi_c^+}} + \frac{\mathcal{G}_3}{M_{\Xi_c^+}} \right] - 3m_\mu^2 (k-1) q^2 Q_- \\
& \times (M_{\Xi_c^+} + M_{\Xi_{cc}^{++}}) \left[\frac{\mathcal{G}_2}{M_{\Xi_{cc}^{++}} + M_{\Xi_c^+}} - \frac{\mathcal{G}_3}{M_{\Xi_c^+}} \right] \Big] + 2q^4 \left[\left(1 - k \frac{M_{\Xi_c^+}}{M_{\Xi_{cc}^{++}}} \right) \mathcal{G}_2 \right. \\
& \left. - \left(1 - k \frac{M_{\Xi_{cc}^{++}}}{M_{\Xi_c^+}} \right) \mathcal{G}_3 \right] \Big\}, \tag{B.2}
\end{aligned}$$

where $\lambda \equiv M_{\Xi_c^+}^4 - 2(M_{\Xi_c^+}^2 + s)M_{\Xi_{cc}^+}^2 + (M_{\Xi_{cc}^+}^2 - s)^2$ and $\tilde{\Omega} \equiv [(M_{\Xi_c^+}^2 - M_{\Xi_{cc}^+}^2)^2 + q^4]$.

$$\begin{aligned}
|\mathcal{A}_k^{(\Xi_{cc}^+, L)}|^2 &= \frac{1}{3q^4}(q^2 - m_\mu^2) \left\{ \left[\mathcal{F}_1^2 + \mathcal{G}_1^2 \right] \left[(2m_\mu^2 + q^2)(M_{\Xi_c^+}^2 - M_{\Xi_{cc}^+}^2)^2 + q^2(q^2 - m_\mu^2) \right. \right. \\
&\quad \times (M_{\Xi_c^+}^2 + M_{\Xi_{cc}^+}^2) - q^4(2q^2 + m_\mu^2) \left. \right] - 6M_{\Xi_c^+}M_{\Xi_{cc}^+}q^4 \left[\mathcal{F}_1^2 - \mathcal{G}_1^2 \right] \left. \right\} + \frac{4}{M_{\Xi_{cc}^+}^2} \\
&\quad \times \left\{ \left[Q_+ \mathcal{F}_2^2 + Q_- \mathcal{G}_2^2 \right] \left[(2m_\mu^2 + q^2)\lambda + 6m_\mu^2 M_{\Xi_{cc}^+}^2 q^2 \right] \right\} + \frac{4}{M_{\Xi_c^+}^2} \left\{ \left[Q_+ \mathcal{F}_3^2 + Q_- \mathcal{G}_3^2 \right] \right. \\
&\quad \times \left[(2m_\mu^2 + q^2)\lambda + 6m_\mu^2 M_{\Xi_c^+}^2 q^2 \right] \left. \right\} + 16 \left\{ -m_\mu^2 q^2 \left[Q_+ \left[\frac{\mathcal{F}_1 \mathcal{F}_2}{M_{\Xi_{cc}^+}} (2M_{\Xi_c^+} - M_{\Xi_{cc}^+}) \right. \right. \right. \\
&\quad \left. \left. \left. - \frac{\mathcal{F}_1 \mathcal{F}_3}{M_{\Xi_c^+}} (M_{\Xi_c^+} - 2M_{\Xi_{cc}^+}) \right] + Q_- \left[\frac{\mathcal{G}_1 \mathcal{G}_2}{M_{\Xi_{cc}^+}} (2M_{\Xi_c^+} + M_{\Xi_{cc}^+}) - \frac{\mathcal{G}_1 \mathcal{G}_3}{M_{\Xi_c^+}} (M_{\Xi_c^+} \right. \right. \right. \\
&\quad \left. \left. \left. + 2M_{\Xi_{cc}^+}) \right] \right] + Q_+ (M_{\Xi_c^+} + M_{\Xi_{cc}^+}) \left[(2m_\mu^2 + q^2)(M_{\Xi_c^+} - M_{\Xi_{cc}^+})^2 - q^4 \right] \left(\frac{\mathcal{F}_1 \mathcal{F}_2}{M_{\Xi_{cc}^+}} \right. \right. \\
&\quad \left. \left. + \frac{\mathcal{F}_1 \mathcal{F}_3}{M_{\Xi_c^+}} \right) + Q_- (M_{\Xi_c^+} - M_{\Xi_{cc}^+}) \left[(2m_\mu^2 + q^2)(M_{\Xi_c^+} + M_{\Xi_{cc}^+})^2 - q^4 \right] \left(\frac{\mathcal{G}_1 \mathcal{G}_2}{M_{\Xi_{cc}^+}} \right. \right. \\
&\quad \left. \left. + \frac{\mathcal{G}_1 \mathcal{G}_3}{M_{\Xi_c^+}} \right) \right\} + \frac{8}{M_{\Xi_c^+} M_{\Xi_{cc}^+}} \left\{ \left[Q_+ \mathcal{F}_2 \mathcal{F}_3 + Q_- \mathcal{G}_2 \mathcal{G}_3 \right] \left[q^4(q^2 - m_\mu^2) - q^2(2q^2 + m_\mu^2) \right. \right. \\
&\quad \times (M_{\Xi_c^+}^2 + M_{\Xi_{cc}^+}^2) + (2m_\mu^2 + q^2)(M_{\Xi_c^+}^2 - M_{\Xi_{cc}^+}^2) \left. \right] \left. \right\} + 32k \left[(2m_\mu^2 + q^2)(M_{\Xi_c^+}^2 \right. \\
&\quad \times \left. - M_{\Xi_{cc}^+}^2 + q^2) + q^2(q^2 - m_\mu^2) \right] \sqrt{\lambda} \mathcal{F}_1 \mathcal{G}_1 + \frac{8k\sqrt{\lambda}}{M_{\Xi_{cc}^+}} \left\{ \left[(M_{\Xi_c^+} - M_{\Xi_{cc}^+})^2 [q^4 \right. \right. \\
&\quad \left. \left. + 2M_{\Xi_{cc}^+}(2m_\mu^2 + q^2)(M_{\Xi_c^+} + M_{\Xi_{cc}^+}) \right] - q^4 [q^2 - m_\mu^2 + 2M_{\Xi_{cc}^+}(M_{\Xi_c^+} + M_{\Xi_{cc}^+})] \right\} \\
&\quad \times \left[\frac{\mathcal{F}_1 \mathcal{G}_2}{M_{\Xi_{cc}^+}} + \frac{\mathcal{F}_1 \mathcal{G}_3}{M_{\Xi_c^+}} \right] - \left[(M_{\Xi_c^+} - M_{\Xi_{cc}^+})^2 [q^4 - 2M_{\Xi_{cc}^+}(2m_\mu^2 + q^2)(M_{\Xi_c^+} - M_{\Xi_{cc}^+}) \right. \\
&\quad \left. - q^4 [q^2 - m_\mu^2 - 2M_{\Xi_{cc}^+}(M_{\Xi_c^+} - M_{\Xi_{cc}^+})] \right] \left[\frac{\mathcal{F}_2 \mathcal{G}_1}{M_{\Xi_{cc}^+}} + \frac{\mathcal{F}_3 \mathcal{G}_1}{M_{\Xi_c^+}} \right] - m_\mu^2 q^2 \left[\frac{\mathcal{F}_1 \mathcal{G}_2}{M_{\Xi_{cc}^+}} \right. \\
&\quad \times \left[(M_{\Xi_c^+} + M_{\Xi_{cc}^+})^2 - 2M_{\Xi_{cc}^+}^2 \right] - \frac{\mathcal{F}_2 \mathcal{G}_1}{M_{\Xi_{cc}^+}} \left[(M_{\Xi_c^+} - M_{\Xi_{cc}^+})^2 - 2M_{\Xi_{cc}^+}^2 \right] + \frac{\mathcal{F}_1 \mathcal{G}_3}{M_{\Xi_c^+}} \\
&\quad \times \left[(M_{\Xi_c^+} - M_{\Xi_{cc}^+})^2 - 2M_{\Xi_{cc}^+}(M_{\Xi_c^+} - 2M_{\Xi_{cc}^+}) \right] - \frac{\mathcal{F}_3 \mathcal{G}_1}{M_{\Xi_c^+}} \left[(M_{\Xi_c^+} + M_{\Xi_{cc}^+})^2 \right. \\
&\quad \left. \left. + 2M_{\Xi_{cc}^+}(M_{\Xi_c^+} + 2M_{\Xi_{cc}^+}) \right] \right] + \frac{q^2(q^2 - m_\mu^2)}{M_{\Xi_c^+} M_{\Xi_{cc}^+}} \left[Q_+ (M_{\Xi_c^+} \mathcal{F}_2 \mathcal{G}_1 + M_{\Xi_{cc}^+} \mathcal{F}_3 \mathcal{G}_1) \right. \\
&\quad \left. - Q_- (M_{\Xi_c^+} \mathcal{F}_1 \mathcal{G}_2 + M_{\Xi_{cc}^+} \mathcal{F}_1 \mathcal{G}_3) \right] \left. \right\} + 8k\sqrt{\lambda} \left\{ (2m_\mu^2 + q^2)\lambda \left(\frac{\mathcal{F}_2 \mathcal{G}_2}{M_{\Xi_{cc}^+}^2} + \frac{\mathcal{F}_3 \mathcal{G}_3}{M_{\Xi_c^+}^2} \right) \right. \\
&\quad \left. + 6m_\mu^2 q^2 (\mathcal{F}_2 \mathcal{G}_2 + \mathcal{F}_3 \mathcal{G}_3) \right\} + \frac{8k\sqrt{\lambda}}{M_{\Xi_c^+} M_{\Xi_{cc}^+}} \left\{ \left[\mathcal{F}_2 \mathcal{G}_3 + \mathcal{F}_3 \mathcal{G}_2 \right] \left[(2m_\mu^2 + q^2)(M_{\Xi_c^+}^2 - M_{\Xi_{cc}^+}^2) \right]^2 \right.
\end{aligned}$$

$$-q^2(M_{\Xi_c^+} + M_{\Xi_{cc}^{++}})(m_\mu^2 + 2q^2) + q^4(q^2 - m_\mu^2)] \Big\} \Big\}. \quad (\text{B.3})$$

$$\begin{aligned}
|\mathcal{A}_k^{(\ell, T)}|^2 &= \frac{1}{3q^4}(q^2 - m_\mu^2) \Big\{ 4 \Big\{ [\mathcal{F}_1^2 + \mathcal{G}_1^2] \Big[(M_{\Xi_c^+}^2 - M_{\Xi_{cc}^{++}}^2) [3\pi k q m_\mu \sqrt{\lambda} + 4(2m_\mu^2 + q^2) \\
&\times (M_{\Xi_c^+}^2 - M_{\Xi_{cc}^{++}}^2)] + 4q^2(q^2 - m_\mu^2)(M_{\Xi_c^+}^2 + M_{\Xi_{cc}^{++}}^2) - 4q^4(2q^2 + m_\mu^2) \Big] \\
&- 24M_{\Xi_c^+} M_{\Xi_{cc}^{++}} q^2 [\mathcal{F}_1^2 - \mathcal{G}_1^2] \Big\} + \frac{1}{M_{\Xi_{cc}^{++}}^2} \Big\{ [Q_+ \mathcal{F}_2^2 + Q_- \mathcal{G}_2^2] [3\pi k q m_\mu \sqrt{\lambda} \\
&\times (M_{\Xi_c^+}^2 - M_{\Xi_{cc}^{++}}^2 - q^2) + 4\lambda(2m_\mu^2 + q^2) + 24m_\mu^2 M_{\Xi_{cc}^{++}}^2 q^2] \Big\} + \frac{1}{M_{\Xi_c^+}^2} \\
&\times \Big\{ [Q_+ \mathcal{F}_3^2 + Q_- \mathcal{G}_3^2] [3\pi k q m_\mu \sqrt{\lambda} (M_{\Xi_c^+}^2 - M_{\Xi_{cc}^{++}}^2 + q^2) + 4\lambda(2m_\mu^2 + q^2) \\
&+ 24m_\mu^2 M_{\Xi_{cc}^{++}}^2 q^2] \Big\} + 4 \Big\{ 3\pi k q m_\mu \lambda \Big[(M_{\Xi_c^+}^2 - M_{\Xi_{cc}^{++}}^2) \Big[(M_{\Xi_c^+} + M_{\Xi_{cc}^{++}}) \Big(\frac{\mathcal{F}_1 \mathcal{F}_2}{M_{\Xi_{cc}^{++}}} \\
&+ \frac{\mathcal{F}_1 \mathcal{F}_3}{M_{\Xi_c^+}} \Big) + (M_{\Xi_c^+} - M_{\Xi_{cc}^{++}}) \Big(\frac{\mathcal{G}_1 \mathcal{G}_2}{M_{\Xi_{cc}^{++}}} + \frac{\mathcal{G}_1 \mathcal{G}_3}{M_{\Xi_c^+}} \Big) \Big] - q^2 \Big(\frac{M_{\Xi_c^+}}{M_{\Xi_{cc}^{++}}} (\mathcal{F}_1 \mathcal{F}_2 + \mathcal{G}_1 \mathcal{G}_2) \\
&- \frac{M_{\Xi_{cc}^{++}}}{M_{\Xi_c^+}} (\mathcal{F}_1 \mathcal{F}_3 + \mathcal{G}_1 \mathcal{G}_3) \Big) \Big] - 4 \Big[Q_+ \Big[m_\mu^2 q^2 \Big(\frac{\mathcal{F}_1 \mathcal{F}_2}{M_{\Xi_{cc}^{++}}} (2M_{\Xi_c^+} - M_{\Xi_{cc}^{++}}) - \frac{\mathcal{F}_1 \mathcal{F}_3}{M_{\Xi_c^+}} \\
&\times (M_{\Xi_c^+} - 2M_{\Xi_{cc}^{++}}) \Big) - (M_{\Xi_c^+} + M_{\Xi_{cc}^{++}}) \Big[(M_{\Xi_c^+} - M_{\Xi_{cc}^{++}})^2 (2m_\mu^2 + q^2) - q^4 \Big] \\
&\times \Big(\frac{\mathcal{F}_1 \mathcal{F}_2}{M_{\Xi_{cc}^{++}}} + \frac{\mathcal{F}_1 \mathcal{F}_3}{M_{\Xi_c^+}} \Big] + Q_- \Big[m_\mu^2 q^2 \Big(\frac{\mathcal{G}_1 \mathcal{G}_2}{M_{\Xi_{cc}^{++}}} (2M_{\Xi_c^+} + M_{\Xi_{cc}^{++}}) - \frac{\mathcal{G}_1 \mathcal{G}_3}{M_{\Xi_c^+}} \\
&\times (M_{\Xi_c^+} + 2M_{\Xi_{cc}^{++}}) \Big) - (M_{\Xi_c^+} - M_{\Xi_{cc}^{++}}) \Big[(M_{\Xi_c^+} + M_{\Xi_{cc}^{++}})^2 (2m_\mu^2 + q^2) - q^4 \Big] \\
&\times \Big(\frac{\mathcal{G}_1 \mathcal{G}_2}{M_{\Xi_{cc}^{++}}} + \frac{\mathcal{G}_1 \mathcal{G}_3}{M_{\Xi_c^+}} \Big) \Big] \Big\} + \frac{2}{M_{\Xi_c^+} M_{\Xi_{cc}^{++}}} \Big\{ [Q_+ \mathcal{F}_2 \mathcal{F}_3 + Q_- \mathcal{G}_2 \mathcal{G}_3] [3\pi k q m_\mu \sqrt{\lambda} \\
&\times (M_{\Xi_c^+}^2 - M_{\Xi_{cc}^{++}}^2) - 4[q^4(q^2 + m_\mu^2) + q^2(M_{\Xi_c^+}^2 + M_{\Xi_{cc}^{++}}^2)(2q^2 - m_\mu^2) \\
&+ (M_{\Xi_c^+}^2 - M_{\Xi_{cc}^{++}}^2)(2m_\mu^2 + q^2)] \Big] \Big\} + 24\pi k q^3 m_\mu \sqrt{\lambda} \mathcal{F}_1 \mathcal{G}_1 \Big\}. \quad (\text{B.4})
\end{aligned}$$

$$\begin{aligned}
|\mathcal{A}_k^{(\Xi_c^+, T)}|^2 &= \frac{1}{3q^4}(q^2 - m_\mu^2) \Big\{ -4 \Big\{ 3\pi k q^3 [Q_- (M_{\Xi_c^+} + M_{\Xi_{cc}^{++}}) \mathcal{F}_1^2 + Q_+ (M_{\Xi_c^+} - M_{\Xi_{cc}^{++}}) \mathcal{G}_1^2] \\
&- 4q^4 \Big[[(M_{\Xi_c^+} - M_{\Xi_{cc}^{++}})^2 - 4M_{\Xi_c^+} M_{\Xi_{cc}^{++}}] \mathcal{F}_1^2 + [(M_{\Xi_c^+} + M_{\Xi_{cc}^{++}})^2 + 4M_{\Xi_c^+} M_{\Xi_{cc}^{++}}] \\
&\times \mathcal{G}_1^2 \Big] + 2 \Big[2q^4(m_\mu^2 + 2q^2) + 2m_\mu^2 q^2 (M_{\Xi_c^+}^2 + M_{\Xi_{cc}^{++}}^2) - (2m_\mu^2 + q^2)(M_{\Xi_c^+}^2 - M_{\Xi_{cc}^{++}}^2) \Big] \\
&\times [\mathcal{F}_1^2 + \mathcal{G}_1^2] \Big\} + \frac{4}{M_{\Xi_{cc}^{++}}^2} \Big\{ [Q_+ \mathcal{F}_2^2 + Q_- \mathcal{G}_2^2] \Big[(2m_\mu^2 + q^2) \lambda + 6m_\mu^2 M_{\Xi_{cc}^{++}}^2 q^2 \Big] \Big\}
\end{aligned}$$

$$\begin{aligned}
& + \frac{4}{M_{\Xi_c^+}^2} \left\{ \left[Q_+ \mathcal{F}_3^2 + Q_- \mathcal{G}_3^2 \right] \left[(2m_\mu^2 + q^2) \lambda + 6m_\mu^2 M_{\Xi_c^+}^2 q^2 \right] \right\} + 2Q_+ \mathcal{F}_1 \\
& \times \left\{ 8m_\mu^2 q^2 \left[\frac{\mathcal{F}_2}{M_{\Xi_{cc}^{++}}} (-2M_{\Xi_c^+} + M_{\Xi_{cc}^{++}}) + \frac{\mathcal{F}_3}{M_{\Xi_c^+}} (M_{\Xi_c^+} - 2M_{\Xi_{cc}^{++}}) \right] - \left[3\pi k q^3 Q_- \right. \right. \\
& - 8(M_{\Xi_c^+} + M_{\Xi_{cc}^{++}}) \left. \left. [(2m_\mu^2 + q^2)(M_{\Xi_c^+} - M_{\Xi_{cc}^{++}})^2 - q^4] \left[\frac{\mathcal{F}_2}{M_{\Xi_{cc}^{++}}} + \frac{\mathcal{F}_3}{M_{\Xi_c^+}} \right] \right] \right\} \\
& - 2Q_- \mathcal{G}_1 \left\{ 8m_\mu^2 q^2 \left[\frac{\mathcal{G}_2}{M_{\Xi_{cc}^{++}}} (2M_{\Xi_c^+} + M_{\Xi_{cc}^{++}}) - \frac{\mathcal{G}_3}{M_{\Xi_c^+}} (M_{\Xi_c^+} + 2M_{\Xi_{cc}^{++}}) \right] + \left[3\pi k q^3 Q_+ \right. \right. \\
& - 8(M_{\Xi_c^+} - M_{\Xi_{cc}^{++}}) \left. \left. [(2m_\mu^2 + q^2)(M_{\Xi_c^+} + M_{\Xi_{cc}^{++}})^2 - q^2] \left[\frac{\mathcal{G}_2}{M_{\Xi_{cc}^{++}}} + \frac{\mathcal{G}_3}{M_{\Xi_c^+}} \right] \right] \right\} \\
& - 24\pi k q M_{\Xi_c^+} m_\mu^2 (M_{\Xi_c^+}^2 - M_{\Xi_{cc}^{++}}^2 - q^2) \mathcal{F}_1 \mathcal{G}_1 + 6\pi k q m_\mu^2 \mathcal{F}_1^2 \left\{ 2q^2 (M_{\Xi_c^+} - M_{\Xi_{cc}^{++}}) \right. \\
& \times \left[\frac{M_{\Xi_c^+}}{M_{\Xi_{cc}^{++}}} \mathcal{G}_2 + \frac{M_{\Xi_{cc}^{++}}}{M_{\Xi_c^+}} \mathcal{G}_3 \right] - (M_{\Xi_c^+}^2 - M_{\Xi_{cc}^{++}}^2) (M_{\Xi_c^+} - M_{\Xi_{cc}^{++}})^2 \left[\frac{\mathcal{G}_2}{M_{\Xi_{cc}^{++}}} + \frac{\mathcal{G}_3}{M_{\Xi_c^+}} \right] \\
& - q^4 \left[\frac{\mathcal{G}_2}{M_{\Xi_{cc}^{++}}} - \frac{\mathcal{G}_3}{M_{\Xi_c^+}} \right] \left. \right\} + 6\pi k q m_\mu^2 \mathcal{G}_1^2 \left\{ 2q^2 (M_{\Xi_c^+} + M_{\Xi_{cc}^{++}}) \left[\frac{M_{\Xi_c^+}}{M_{\Xi_{cc}^{++}}} \mathcal{F}_2 - \frac{M_{\Xi_{cc}^{++}}}{M_{\Xi_c^+}} \mathcal{F}_3 \right] \right. \\
& \left. - (M_{\Xi_c^+}^2 - M_{\Xi_{cc}^{++}}^2) (M_{\Xi_c^+} + M_{\Xi_{cc}^{++}})^2 \left[\frac{\mathcal{F}_2}{M_{\Xi_{cc}^{++}}} + \frac{\mathcal{F}_3}{M_{\Xi_c^+}} \right] - q^4 \left[\frac{\mathcal{F}_2}{M_{\Xi_{cc}^{++}}} - \frac{\mathcal{F}_3}{M_{\Xi_c^+}} \right] \right\} \left. \right\}. \tag{B.5}
\end{aligned}$$

$$\begin{aligned}
|\mathcal{A}_k^{(\Xi_{cc}^{++}, T)}|^2 &= \frac{1}{3q^4} (q^2 - m_\mu^2) \left\{ 4 \left\{ 3\pi k q^3 \left[-Q_- (M_{\Xi_c^+} + M_{\Xi_{cc}^{++}}) \mathcal{F}_1^2 + Q_+ (M_{\Xi_c^+} - M_{\Xi_{cc}^{++}}) \mathcal{G}_1^2 \right] \right. \right. \\
& + 4 \left[\mathcal{F}_1^2 + \mathcal{G}_1^2 \right] \left[(2m_\mu^2 + q^2) (M_{\Xi_c^+}^2 - M_{\Xi_{cc}^{++}}^2) + q^2 (q^2 - m_\mu^2) (M_{\Xi_c^+}^2 + M_{\Xi_{cc}^{++}}^2) \right. \\
& \left. \left. - q^4 (2q^2 + m_\mu^2) \right] - 24M_{\Xi_c^+} M_{\Xi_{cc}^{++}} q^4 \left[\mathcal{F}_1^2 - \mathcal{G}_1^2 \right] \right\} + \frac{4}{M_{\Xi_{cc}^{++}}^2} \left\{ \left[Q_+ \mathcal{F}_2^2 + Q_- \mathcal{G}_2^2 \right] \right. \\
& \times \left[(2m_\mu^2 + q^2) \lambda + 6m_\mu^2 M_{\Xi_{cc}^{++}}^2 q^2 \right] \left. \right\} + \frac{4}{M_{\Xi_c^+}^2} \left\{ \left[Q_+ \mathcal{F}_3^2 + Q_- \mathcal{G}_3^2 \right] \left[(2m_\mu^2 + q^2) \lambda \right. \right. \\
& + 6m_\mu^2 M_{\Xi_c^+}^2 q^2 \left. \left. \right\} - 2 \left\{ 3\pi k q^3 \lambda \left[\frac{1}{M_{\Xi_{cc}^{++}}} \left[\mathcal{F}_1 \mathcal{F}_2 - \mathcal{G}_1 \mathcal{G}_2 \right] + \frac{1}{M_{\Xi_c^+}} \left[\mathcal{F}_1 \mathcal{F}_3 - \mathcal{G}_1 \mathcal{G}_3 \right] \right] \right. \right. \\
& + 8m_\mu^2 q^2 \left[Q_+ \left[\frac{\mathcal{F}_1 \mathcal{F}_2}{M_{\Xi_{cc}^{++}}} (2M_{\Xi_c^+} - M_{\Xi_{cc}^{++}}) - \frac{\mathcal{F}_1 \mathcal{F}_3}{M_{\Xi_c^+}} (M_{\Xi_c^+} - 2M_{\Xi_{cc}^{++}}) \right] + Q_- \left[\frac{\mathcal{G}_1 \mathcal{G}_2}{M_{\Xi_{cc}^{++}}} \right. \right. \\
& \times (2M_{\Xi_c^+} + M_{\Xi_{cc}^{++}}) - \frac{\mathcal{G}_1 \mathcal{G}_3}{M_{\Xi_c^+}} (M_{\Xi_c^+} + 2M_{\Xi_{cc}^{++}}) \left. \left. \right] \right] - 8Q_+ (M_{\Xi_c^+} + M_{\Xi_{cc}^{++}}) \left[(2m_\mu^2 + q^2) \right. \\
& \times (M_{\Xi_c^+} - M_{\Xi_{cc}^{++}})^2 - q^4 \left(\frac{\mathcal{F}_1 \mathcal{F}_2}{M_{\Xi_{cc}^{++}}} + \frac{\mathcal{F}_1 \mathcal{F}_3}{M_{\Xi_c^+}} \right) - 8Q_- (M_{\Xi_c^+} - M_{\Xi_{cc}^{++}}) \left[(2m_\mu^2 + q^2) \right. \\
& \times (M_{\Xi_c^+} + M_{\Xi_{cc}^{++}})^2 - q^4 \left(\frac{\mathcal{G}_1 \mathcal{G}_2}{M_{\Xi_{cc}^{++}}} + \frac{\mathcal{G}_1 \mathcal{G}_3}{M_{\Xi_c^+}} \right) \left. \right\} + \frac{8}{M_{\Xi_c^+} M_{\Xi_{cc}^{++}}} \left\{ \left[Q_+ \mathcal{F}_2 \mathcal{F}_3 \right. \right. \\
& + Q_- \mathcal{G}_2 \mathcal{G}_3 \left. \left. \right] \left[(2m_\mu^2 + q^2) (M_{\Xi_c^+}^2 - M_{\Xi_{cc}^{++}}^2) - q^2 (2q^2 + m_\mu^2) (M_{\Xi_c^+}^2 + M_{\Xi_{cc}^{++}}^2) \right] \right\}.
\end{aligned}$$

$$\begin{aligned}
& + q^4(q^2 - m_\mu^2) \Big] \Big\} - 24\pi kq M_{\Xi_{cc}^{++}} m_\mu^2 (M_{\Xi_c^+}^2 - M_{\Xi_{cc}^{++}}^2 + q^2) \mathcal{F}_1 \mathcal{G}_1 + 6\pi kq m_\mu^2 \\
& \times \left\{ q^4 \left[\frac{1}{M_{\Xi_{cc}^{++}}} [\mathcal{F}_1 \mathcal{G}_2 - \mathcal{F}_2 \mathcal{G}_1] - \frac{1}{M_{\Xi_c^+}} [\mathcal{F}_1 \mathcal{G}_3 - \mathcal{F}_3 \mathcal{G}_1] \right] - 2q^2 \left[(M_{\Xi_c^+} - M_{\Xi_{cc}^{++}}) \right. \right. \\
& \times \left(\frac{M_{\Xi_c^+}}{M_{\Xi_{cc}^{++}}} \mathcal{F}_1 \mathcal{G}_2 + \frac{M_{\Xi_{cc}^{++}}}{M_{\Xi_c^+}} \mathcal{F}_1 \mathcal{G}_3 \right) + (M_{\Xi_c^+} + M_{\Xi_{cc}^{++}}) \left(-\frac{M_{\Xi_c^+}}{M_{\Xi_{cc}^{++}}} \mathcal{F}_2 \mathcal{G}_1 \right. \\
& \left. \left. + \frac{M_{\Xi_{cc}^{++}}}{M_{\Xi_c^+}} \mathcal{F}_3 \mathcal{G}_1 \right) \right] + (M_{\Xi_c^+}^2 - M_{\Xi_{cc}^{++}}^2) \left[(M_{\Xi_c^+} - M_{\Xi_{cc}^{++}})^2 \left(\frac{\mathcal{F}_1 \mathcal{G}_2}{M_{\Xi_{cc}^{++}}} + \frac{\mathcal{F}_1 \mathcal{G}_3}{M_{\Xi_c^+}} \right) \right. \\
& \left. \left. - (M_{\Xi_c^+} + M_{\Xi_{cc}^{++}})^2 \left(\frac{\mathcal{F}_2 \mathcal{G}_1}{M_{\Xi_{cc}^{++}}} + \frac{\mathcal{F}_3 \mathcal{G}_1}{M_{\Xi_c^+}} \right) \right] \right\}. \tag{B.6}
\end{aligned}$$

References

- [1] M. Gell-Mann, *A Schematic Model of Baryons and Mesons*, *Phys. Lett.* **8** (1964) 214.
- [2] SELEX collaboration, *First Observation of the Doubly Charmed Baryon Ξ_{cc}^+* , *Phys. Rev. Lett.* **89** (2002) 112001 [[hep-ex/0208014](#)].
- [3] LHCb collaboration, *Observation of the doubly charmed baryon Ξ_{cc}^{++}* , *Phys. Rev. Lett.* **119** (2017) 112001 [[arXiv:1707.01621](#)].
- [4] LHCb collaboration, *Search for the doubly charmed baryon Ξ_{cc}^+* , *Sci. China Phys. Mech. Astron.* **63** (2020) 221062 [[arXiv:1909.12273](#)].
- [5] LHCb collaboration, *Search for the doubly charmed baryon Ξ_{cc}^+ in the $\Xi_c^+ \pi^- \pi^+$ final state*, *JHEP* **12** (2021) 107 [[arXiv:2109.07292](#)].
- [6] LHCb collaboration, *Search for the doubly heavy baryons Ω_{bc}^0 and Ξ_{bc}^0 decaying to $\Lambda_c^+ \pi^-$ and $\Xi_c^+ \pi^-$* , *Chin. Phys. C* **45** (2021) 093002 [[arXiv:2104.04759](#)].
- [7] M. Shekari Tousi and K. Azizi, *Properties of doubly heavy spin- $\frac{1}{2}$ baryons: The ground and excited states*, *Phys. Rev. D* **109** (2024) 054005 [[arXiv:2401.07151](#)].
- [8] T.M. Aliev, K. Azizi and M. Savci, *Doubly Heavy Spin-1/2 Baryon Spectrum in QCD*, *Nucl. Phys. A* **895** (2012) 59 [[arXiv:1205.2873](#)].
- [9] T.M. Aliev, K. Azizi and M. Savci, *The masses and residues of doubly heavy spin-3/2 baryons*, *J. Phys. G* **40** (2013) 065003 [[arXiv:1208.1976](#)].
- [10] T.M. Aliev and S. Bilmis, *The mass and residues of radially and orbitally excited doubly heavy baryons in QCD*, *Nucl. Phys. A* **984** (2019) 99 [[arXiv:1904.11279](#)].
- [11] T. Aliyev and S. Bilmiş, *Properties of doubly heavy baryons in QCD*, *Turk. J. Phys.* **46** (2022) 1 [[arXiv:2203.02965](#)].
- [12] Q.-F. Lü, K.-L. Wang, L.-Y. Xiao and X.-H. Zhong, *Mass spectra and radiative transitions of doubly heavy baryons in a relativized quark model*, *Phys. Rev. D* **96** (2017) 114006 [[arXiv:1708.04468](#)].
- [13] Z.-G. Wang, *Analysis of the doubly heavy baryon states and pentaquark states with QCD sum rules*, *Eur. Phys. J. C* **78** (2018) 826 [[arXiv:1808.09820](#)].
- [14] D. Ebert, R.N. Faustov, V.O. Galkin and A.P. Martynenko, *Mass spectra of doubly heavy baryons in the relativistic quark model*, *Phys. Rev. D* **66** (2002) 014008 [[hep-ph/0201217](#)].

- [15] J.-R. Zhang and M.-Q. Huang, *Doubly heavy baryons in QCD sum rules*, *Phys. Rev. D* **78** (2008) 094007 [[arXiv:0810.5396](#)].
- [16] Z.-G. Wang, *Analysis of the $\frac{1}{2}^+$ doubly heavy baryon states with QCD sum rules*, *Eur. Phys. J. A* **45** (2010) 267 [[arXiv:1001.4693](#)].
- [17] S. Rahmani, H. Hassanabadi and H. Sobhani, *Mass and decay properties of double heavy baryons with a phenomenological potential model*, *Eur. Phys. J. C* **80** (2020) 312.
- [18] D.-L. Yao, *Masses and sigma terms of doubly charmed baryons up to $\mathcal{O}(p^4)$ in manifestly Lorentz-invariant baryon chiral perturbation theory*, *Phys. Rev. D* **97** (2018) 034012 [[arXiv:1801.09462](#)].
- [19] M. Padmanath, *Heavy baryon spectroscopy from lattice QCD*, 5, 2019 [[arXiv:1905.10168](#)].
- [20] Z.S. Brown, W. Detmold, S. Meinel and K. Orginos, *Charmed bottom baryon spectroscopy from lattice QCD*, *Phys. Rev. D* **90** (2014) 094507 [[arXiv:1409.0497](#)].
- [21] Z. Shah and A.K. Rai, *Excited state mass spectra of doubly heavy Ξ baryons*, *Eur. Phys. J. C* **77** (2017) 129 [[arXiv:1702.02726](#)].
- [22] F. Giannuzzi, *Doubly heavy baryons in a Salpeter model with AdS/QCD inspired potential*, *Phys. Rev. D* **79** (2009) 094002 [[arXiv:0902.4624](#)].
- [23] Z. Shah, K. Thakkar and A.K. Rai, *Excited State Mass spectra of doubly heavy baryons Ω_{cc} , Ω_{bb} and Ω_{bc}* , *Eur. Phys. J. C* **76** (2016) 530 [[arXiv:1609.03030](#)].
- [24] A. Valcarce, H. Garcilazo and J. Vijande, *Towards an understanding of heavy baryon spectroscopy*, *Eur. Phys. J. A* **37** (2008) 217 [[arXiv:0807.2973](#)].
- [25] Z.-G. Wang, *Analysis of the $1/2^-$ and $3/2^-$ heavy and doubly heavy baryon states with QCD sum rules*, *Eur. Phys. J. A* **47** (2011) 81 [[arXiv:1003.2838](#)].
- [26] T. Yoshida, E. Hiyama, A. Hosaka, M. Oka and K. Sadato, *Spectrum of heavy baryons in the quark model*, *Phys. Rev. D* **92** (2015) 114029 [[arXiv:1510.01067](#)].
- [27] E. Ortiz-Pacheco and R. Bijker, *Masses and radiative decay widths of S- and P-wave singly, doubly, and triply heavy charm and bottom baryons*, *Phys. Rev. D* **108** (2023) 054014 [[arXiv:2307.04939](#)].
- [28] P.-C. Qiu and D.-L. Yao, *Chiral effective Lagrangian for doubly charmed baryons up to $\mathcal{O}(q^4)$* , *Phys. Rev. D* **103** (2021) 034006 [[arXiv:2012.11117](#)].
- [29] T.M. Aliev, K. Azizi and M. Savcı, *Mixing angle of doubly heavy baryons in QCD*, *Phys. Lett. B* **715** (2012) 149 [[arXiv:1205.6320](#)].
- [30] T.M. Aliev and K. Şimşek, *Strong coupling constants of doubly heavy baryons with vector mesons in QCD*, *Eur. Phys. J. C* **80** (2020) 976 [[arXiv:2009.03464](#)].
- [31] A.R. Olamaei, K. Azizi and S. Rostami, *Strong coupling constants of the doubly heavy Ξ_{QQ} Baryons with π Meson*, *Eur. Phys. J. C* **80** (2020) 613 [[arXiv:2003.12723](#)].
- [32] T.M. Aliev and K. Şimşek, *Strong vertices of doubly heavy spin- 3/2 –spin- 1/2 baryons with light mesons in light-cone QCD sum rules*, *Phys. Rev. D* **103** (2021) 054044 [[arXiv:2011.07150](#)].
- [33] T.M. Aliev, T. Barakat and K. Şimşek, *Strong $B_{QQ}^* B_{QQ} V$ vertices and the radiative decays of $B_{QQ}^* \rightarrow B_{QQ} \gamma$ in the light-cone sum rules*, *Eur. Phys. J. A* **57** (2021) 160 [[arXiv:2101.10264](#)].

- [34] A.R. Olamaei, K. Azizi and S. Rostami, *Strong vertices of doubly heavy spin-3/2 baryons with light pseudoscalar mesons*, *Chin. Phys. C* **45** (2021) 113107 [[arXiv:2102.03852](#)].
- [35] H.I. Alrebdi, T.M. Aliev and K. Şimşek, *Determination of the strong vertices of doubly heavy baryons with pseudoscalar mesons in QCD*, *Phys. Rev. D* **102** (2020) 074007 [[arXiv:2008.05098](#)].
- [36] K. Azizi, A.R. Olamaei and S. Rostami, *Strong interaction of doubly heavy spin-3/2 baryons with light vector mesons*, *Eur. Phys. J. C* **80** (2020) 1196 [[arXiv:2011.02919](#)].
- [37] Q. Qin, Y.-J. Shi, W. Wang, G.-H. Yang, F.-S. Yu and R. Zhu, *Inclusive approach to hunt for the beauty-charmed baryons Ξ_{bc}* , *Phys. Rev. D* **105** (2022) L031902 [[arXiv:2108.06716](#)].
- [38] L.-Y. Xiao, K.-L. Wang, Q.-f. Lu, X.-H. Zhong and S.-L. Zhu, *Strong and radiative decays of the doubly charmed baryons*, *Phys. Rev. D* **96** (2017) 094005 [[arXiv:1708.04384](#)].
- [39] L.-Y. Xiao, Q.-F. Lü and S.-L. Zhu, *Strong decays of the 1P and 2D doubly charmed states*, *Phys. Rev. D* **97** (2018) 074005 [[arXiv:1712.07295](#)].
- [40] H.-S. Li, L. Meng, Z.-W. Liu and S.-L. Zhu, *Radiative decays of the doubly charmed baryons in chiral perturbation theory*, *Phys. Lett. B* **777** (2018) 169 [[arXiv:1708.03620](#)].
- [41] Z.-X. Zhao, *Weak decays of doubly heavy baryons: the 1/2 \rightarrow 3/2 case*, *Eur. Phys. J. C* **78** (2018) 756 [[arXiv:1805.10878](#)].
- [42] Z.-P. Xing and Z.-X. Zhao, *Weak decays of doubly heavy baryons: the FCNC processes*, *Phys. Rev. D* **98** (2018) 056002 [[arXiv:1807.03101](#)].
- [43] L.-J. Jiang, B. He and R.-H. Li, *Weak decays of doubly heavy baryons: $\mathcal{B}_{cc} \rightarrow \mathcal{B}_c V$* , *Eur. Phys. J. C* **78** (2018) 961 [[arXiv:1810.00541](#)].
- [44] M.S. Tousi, K. Azizi and H.R. Moshfegh, *Investigation of the semileptonic decay $\Xi_{cc}^{++} \rightarrow \Xi_c^+ \bar{\ell} \nu_\ell$ within QCD sum rules*, *Phys. Rev. D* **110** (2024) 114001 [[arXiv:2409.00241](#)].
- [45] A.S. Gerasimov and A.V. Luchinsky, *Weak decays of doubly heavy baryons: Decays to a system of π mesons*, *Phys. Rev. D* **100** (2019) 073015 [[arXiv:1905.11740](#)].
- [46] W. Wang, F.-S. Yu and Z.-X. Zhao, *Weak decays of doubly heavy baryons: the 1/2 \rightarrow 1/2 case*, *Eur. Phys. J. C* **77** (2017) 781 [[arXiv:1707.02834](#)].
- [47] N. Sharma and R. Dhir, *Estimates of W-exchange contributions to Ξ_{cc} decays*, *Phys. Rev. D* **96** (2017) 113006 [[arXiv:1709.08217](#)].
- [48] K. Patel and K. Thakkar, *Transition Properties of Doubly Heavy Baryons*, *Int. J. Theor. Phys.* **64** (2025) 129 [[arXiv:2408.00335](#)].
- [49] T. Gutsche, M.A. Ivanov, J.G. Körner and V.E. Lyubovitskij, *Novel ideas in nonleptonic decays of double heavy baryons*, *Particles* **2** (2019) 339 [[arXiv:1905.06219](#)].
- [50] T. Gutsche, M.A. Ivanov, J.G. Körner, V.E. Lyubovitskij and Z. Tyulemissov, *Analysis of the semileptonic and nonleptonic two-body decays of the double heavy charm baryon states Ξ_{cc}^{++} , Ξ_{cc}^+ and Ω_{cc}^+* , *Phys. Rev. D* **100** (2019) 114037 [[arXiv:1911.10785](#)].
- [51] H.-W. Ke, F. Lu, X.-H. Liu and X.-Q. Li, *Study on $\Xi_{cc} \rightarrow \Xi_c$ and $\Xi_{cc} \rightarrow \Xi_c'$ weak decays in the light-front quark model*, *Eur. Phys. J. C* **80** (2020) 140 [[arXiv:1912.01435](#)].
- [52] H.-Y. Cheng, G. Meng, F. Xu and J. Zou, *Two-body weak decays of doubly charmed baryons*, *Phys. Rev. D* **101** (2020) 034034 [[arXiv:2001.04553](#)].

- [53] X.-H. Hu, R.-H. Li and Z.-P. Xing, *A comprehensive analysis of weak transition form factors for doubly heavy baryons in the light front approach*, *Eur. Phys. J. C* **80** (2020) 320 [[arXiv:2001.06375](#)].
- [54] R.-H. Li, J.-J. Hou, B. He and Y.-R. Wang, *Weak Decays of Doubly Heavy Baryons: $\mathcal{B}_{cc} \rightarrow \mathcal{B}D^{(*)}$* , *Chin. Phys. C* **45** (2021) 043108 [[arXiv:2010.09362](#)].
- [55] J.-J. Han, R.-X. Zhang, H.-Y. Jiang, Z.-J. Xiao and F.-S. Yu, *Weak decays of bottom-charm baryons: $\mathcal{B}_{bc} \rightarrow \mathcal{B}_b P$* , *Eur. Phys. J. C* **81** (2021) 539 [[arXiv:2102.00961](#)].
- [56] W. Wang, Z.-P. Xing and J. Xu, *Weak Decays of Doubly Heavy Baryons: $SU(3)$ Analysis*, *Eur. Phys. J. C* **77** (2017) 800 [[arXiv:1707.06570](#)].
- [57] Y.-J. Shi, W. Wang, Y. Xing and J. Xu, *Weak Decays of Doubly Heavy Baryons: Multi-body Decay Channels*, *Eur. Phys. J. C* **78** (2018) 56 [[arXiv:1712.03830](#)].
- [58] M.A. Ivanov, J.G. Körner and V.E. Lyubovitskij, *Nonleptonic Decays of Doubly Charmed Baryons*, *Phys. Part. Nucl.* **51** (2020) 678.
- [59] Y.-J. Shi, W. Wang, Z.-X. Zhao and U.-G. Meißner, *Towards a Heavy Diquark Effective Theory for Weak Decays of Doubly Heavy Baryons*, *Eur. Phys. J. C* **80** (2020) 398 [[arXiv:2002.02785](#)].
- [60] X.-H. Hu, Y.-L. Shen, W. Wang and Z.-X. Zhao, *Weak decays of doubly heavy baryons: "decay constants"*, *Chin. Phys. C* **42** (2018) 123102 [[arXiv:1711.10289](#)].
- [61] R.-H. Li and C.-D. Lu, *Search for doubly heavy baryon via weak decays*, in *53rd Rencontres de Moriond on QCD and High Energy Interactions*, p. 115, 2018 [[arXiv:1805.09064](#)].
- [62] Y.-J. Shi, W. Wang and Z.-X. Zhao, *QCD Sum Rules Analysis of Weak Decays of Doubly-Heavy Baryons*, *Eur. Phys. J. C* **80** (2020) 568 [[arXiv:1902.01092](#)].
- [63] Y.-J. Shi, Y. Xing and Z.-X. Zhao, *Light-cone sum rules analysis of $\Xi_{QQ'q} \rightarrow \Lambda_{Q'}$ weak decays*, *Eur. Phys. J. C* **79** (2019) 501 [[arXiv:1903.03921](#)].
- [64] T. Gutsche, M.A. Ivanov, J.G. Körner and V.E. Lyubovitskij, *Decay chain information on the newly discovered double charm baryon state Ξ_{cc}^{++}* , *Phys. Rev. D* **96** (2017) 054013 [[arXiv:1708.00703](#)].
- [65] T. Gutsche, M.A. Ivanov, J.G. Körner, V.E. Lyubovitskij and Z. Tyulemissov, *Ab initio three-loop calculation of the W -exchange contribution to nonleptonic decays of double charm baryons*, *Phys. Rev. D* **99** (2019) 056013 [[arXiv:1812.09212](#)].
- [66] M. Shekari Tousi and K. Azizi, *Semileptonic decays of doubly charmed or bottom baryons to single heavy baryons*, *Phys. Rev. D* **112** (2025) 074012 [[arXiv:2504.17030](#)].
- [67] U. Özdem, *Magnetic moments of doubly heavy baryons in light-cone QCD*, *J. Phys. G* **46** (2019) 035003 [[arXiv:1804.10921](#)].
- [68] U. Özdem, *Magnetic dipole moments of the spin- $\frac{3}{2}$ doubly heavy baryons*, *Eur. Phys. J. A* **56** (2020) 34 [[arXiv:1906.08353](#)].
- [69] A.V. Berezhnoy, A.K. Likhoded and A.V. Luchinsky, *Doubly heavy baryons at the LHC*, *Phys. Rev. D* **98** (2018) 113004 [[arXiv:1809.10058](#)].
- [70] M.A. Shifman, A.I. Vainshtein and V.I. Zakharov, *QCD and Resonance Physics. Theoretical Foundations*, *Nucl. Phys. B* **147** (1979) 385.
- [71] M.A. Shifman, A.I. Vainshtein and V.I. Zakharov, *QCD and Resonance Physics: Applications*, *Nucl. Phys. B* **147** (1979) 448.

- [72] T.M. Aliev, K. Azizi and M. Savci, *Analysis of the $\Lambda_b \rightarrow \Lambda \ell^+ \ell^-$ decay in QCD*, *Phys. Rev. D* **81** (2010) 056006 [[arXiv:1001.0227](#)].
- [73] T.M. Aliev, K. Azizi and A. Ozpineci, *Radiative Decays of the Heavy Flavored Baryons in Light Cone QCD Sum Rules*, *Phys. Rev. D* **79** (2009) 056005 [[arXiv:0901.0076](#)].
- [74] S.S. Agaev, K. Azizi and H. Sundu, *Strong $Z_c^+(3900) \rightarrow J/\psi \pi^+; \eta_c \rho^+$ decays in QCD*, *Phys. Rev. D* **93** (2016) 074002 [[arXiv:1601.03847](#)].
- [75] K. Azizi, Y. Sarac and H. Sundu, *Analysis of $P_c^+(4380)$ and $P_c^+(4450)$ as pentaquark states in the molecular picture with QCD sum rules*, *Phys. Rev. D* **95** (2017) 094016 [[arXiv:1612.07479](#)].
- [76] Y.-M. Wang, H. Zou, Z.-T. Wei, X.-Q. Li and C.-D. Lu, *The Transition form-factors for semi-leptonic weak decays of J/ψ in QCD sum rules*, *Eur. Phys. J. C* **54** (2008) 107 [[arXiv:0707.1138](#)].
- [77] M. Shekari Tousi and K. Azizi, *Examining possible doubly topped baryon configurations*, [arXiv:2601.11985](#).
- [78] T.M. Aliev, E. Askan and A. Ozpineci, *Multipole moments of double heavy $J^P = \frac{3}{2}^+$ baryons*, *Eur. Phys. J. C* **85** (2025) 1479 [[arXiv:2504.10199](#)].
- [79] Z. Neishabouri and K. Azizi, *Investigation of the semileptonic decays $\Xi_b^{(\prime)} \rightarrow \Xi_c^{(\prime)} \ell \bar{\nu}_\ell$* , *Phys. Rev. D* **112** (2025) 054009 [[arXiv:2503.12390](#)].
- [80] J. Lu, G.-L. Yu, D.-Y. Chen, Z.-G. Wang and B. Wu, *Analysis of the semileptonic decays $\Lambda_b \rightarrow \Lambda_c \ell \bar{\nu}_\ell$ and $\Xi_b \rightarrow \Xi_c \ell \bar{\nu}_\ell$ in QCD sum rules*, *Eur. Phys. J. C* **85** (2025) 1382 [[arXiv:2508.11900](#)].
- [81] M. Ahmadi, Z.R. Najjar and K. Azizi, *Study of the semileptonic decay $\Lambda \rightarrow p \ell \bar{\nu}_\ell$ in QCD*, *Phys. Rev. D* **112** (2025) 094035 [[arXiv:2509.23421](#)].
- [82] G.-L. Yu, Z.-G. Wang, J. Lu, B. Wu, P. Yang and Z. Zhou, *Analysis of the semileptonic decays of Ξ_{cc} and Ω_{cc} baryons in QCD sum rules*, [arXiv:2601.06427](#).
- [83] A. Crivellin, C. Greub and A. Kokulu, *Explaining $B \rightarrow D \tau \nu$, $B \rightarrow D^* \tau \nu$ and $B \rightarrow \tau \nu$ in a 2HDM of type III*, *Phys. Rev. D* **86** (2012) 054014 [[arXiv:1206.2634](#)].
- [84] Y. Sakaki and H. Tanaka, *Constraints on the charged scalar effects using the forward-backward asymmetry on $B \rightarrow D^{(*)} \tau \bar{\nu}_\tau$* , *Phys. Rev. D* **87** (2013) 054002 [[arXiv:1205.4908](#)].
- [85] Y. Sakaki, M. Tanaka, A. Tayduganov and R. Watanabe, *Probing New Physics with q^2 distributions in $\bar{B} \rightarrow D^{(*)} \tau \bar{\nu}$* , *Phys. Rev. D* **91** (2015) 114028 [[arXiv:1412.3761](#)].
- [86] L. Calibbi, A. Crivellin and T. Ota, *Effective Field Theory Approach to $b \rightarrow s \ell \ell^{(\prime)}$, $B \rightarrow K^{(*)} \nu \bar{\nu}$ and $B \rightarrow D^{(*)} \tau \nu$ with Third Generation Couplings*, *Phys. Rev. Lett.* **115** (2015) 181801 [[arXiv:1506.02661](#)].
- [87] B. Dumont, K. Nishiwaki and R. Watanabe, *LHC constraints and prospects for S_1 scalar leptoquark explaining the $\bar{B} \rightarrow D^{(*)} \tau \bar{\nu}$ anomaly*, *Phys. Rev. D* **94** (2016) 034001 [[arXiv:1603.05248](#)].
- [88] F. Feruglio, P. Paradisi and A. Pattori, *Revisiting Lepton Flavor Universality in B Decays*, *Phys. Rev. Lett.* **118** (2017) 011801 [[arXiv:1606.00524](#)].
- [89] M. Bordone, G. Isidori and A. Pattori, *On the Standard Model predictions for R_K and R_{K^*}* , *Eur. Phys. J. C* **76** (2016) 440 [[arXiv:1605.07633](#)].

- [90] M. Bordone, G. Isidori and S. Trifinopoulos, *Semileptonic B-physics anomalies: A general EFT analysis within $U(2)^n$ flavor symmetry*, *Phys. Rev. D* **96** (2017) 015038 [[arXiv:1702.07238](#)].
- [91] D. Choudhury, A. Kundu, R. Mandal and R. Sinha, *Minimal unified resolution to $R_{K^{(*)}}$ and $R(D^{(*)})$ anomalies with lepton mixing*, *Phys. Rev. Lett.* **119** (2017) 151801 [[arXiv:1706.08437](#)].
- [92] S.-P. Li, X.-Q. Li, Y.-D. Yang and X. Zhang, *$R_{D^{(*)}}, R_{K^{(*)}}$ and neutrino mass in the 2HDM-III with right-handed neutrinos*, *JHEP* **09** (2018) 149 [[arXiv:1807.08530](#)].
- [93] Z. Aarfi, Q.M.U. Salam, I. Ahmed, F.M. Bhutta, R. Khalid and M.A. Paracha, *Investigating New Physics through the Observables of Semileptonic $B_s \rightarrow K^*(\rightarrow K\pi)\mu^+\mu^-$ Decay*, *PTEP* **2025** (2025) 123 [[arXiv:2506.20446](#)].
- [94] Q.M.U. Salam, I. Ahmed, R. Khalid and I.U. Rehman, *Exploring new physics in transition $b \rightarrow s\ell^+\ell^-$ through different $B_c \rightarrow D_s^{(*)}\ell^+\ell^-$ observables*, *J. Phys. G* **52** (2025) 045003 [[arXiv:2411.00912](#)].
- [95] S.-W. Wang, $\Xi_b \rightarrow \Xi_c\tau\bar{\nu}_\tau$ decay in new physics models, *Int. J. Theor. Phys.* **60** (2021) 982.
- [96] D.-Y. Wang, Y.-D. Yang and X.-B. Yuan, $b \rightarrow c\tau\bar{\nu}$ decays in supersymmetry with R-parity violation, *Chin. Phys. C* **43** (2019) 083103 [[arXiv:1905.08784](#)].
- [97] J.D. Gómez, N. Quintero and E. Rojas, *Charged current $b \rightarrow c\tau\bar{\nu}_\tau$ anomalies in a general W' boson scenario*, *Phys. Rev. D* **100** (2019) 093003 [[arXiv:1907.08357](#)].
- [98] T. Yasmeen, I. Ahmed, S. Shafaq, M. Arslan and M.J. Aslam, *Probing New Physics in Light of Recent Developments in $b \rightarrow c\ell\nu$ Transitions*, *PTEP* **2024** (2024) 073B07 [[arXiv:2401.02334](#)].
- [99] C. Bolognani, M. Reboud, D. van Dyk and K.K. Vos, *Constraining $|V_{cs}|$ and physics beyond the Standard Model from exclusive (semi)leptonic charm decays*, *JHEP* **09** (2024) 099 [[arXiv:2407.06145](#)].
- [100] S. Fajfer, I. Nisandzic and U. Rojcek, *Discerning new physics in charm meson leptonic and semileptonic decays*, *Phys. Rev. D* **91** (2015) 094009 [[arXiv:1502.07488](#)].
- [101] X. Leng, X.-L. Mu, Z.-T. Zou and Y. Li, *Investigation on effects of new physics in $c \rightarrow (s, d)\ell^+\nu_\ell$ transitions*, *Chin. Phys. C* **45** (2021) 063107 [[arXiv:2011.01061](#)].
- [102] Z.-H. Zhang and Y. Li, *Investigation of $\Lambda_c \rightarrow (\Lambda, n)\ell^+\nu_\ell$ decays in the standard model and beyond*, *Phys. Rev. D* **111** (2025) 053008 [[arXiv:2501.12871](#)].
- [103] BESIII collaboration, *Observation of $D_s^+ \rightarrow \eta'\mu^+\nu_\mu$, Precision Test of Lepton Flavor Universality with $D_s^+ \rightarrow \eta^{(\prime)}\ell^+\nu_\ell$, and First Measurements of $D_s^+ \rightarrow \eta^{(\prime)}\mu^+\nu_\mu$ Decay Dynamics*, *Phys. Rev. Lett.* **132** (2024) 091802 [[arXiv:2307.12852](#)].
- [104] S. Zafar, Q.M.U. Salam, R. Khan, I. Ahmed and R. Khalid, *Chirality structure of vector like new physics operators in charged current transitions*, *Eur. Phys. J. Plus* **140** (2025) 1167 [[arXiv:2507.23721](#)].
- [105] P. Colangelo, F. De Fazio and F. Loporco, *Role of $B_c^+ \rightarrow B_{s,d}^{(*)}\bar{\ell}\nu_\ell$ in the Standard Model and in the search for BSM signals*, *Phys. Rev. D* **103** (2021) 075019 [[arXiv:2102.05365](#)].
- [106] B. Belfatto, R. Beradze and Z. Berezhiani, *The CKM unitarity problem: A trace of new physics at the TeV scale?*, *Eur. Phys. J. C* **80** (2020) 149 [[arXiv:1906.02714](#)].

- [107] P. Boora, D. Kumar and K. Lalwani, *New physics effects with right-handed neutrinos in semileptonic decay $B_c^+ \rightarrow B_s \mu^+ \nu_\mu$* , *Eur. Phys. J. C* **85** (2025) 370 [[arXiv:2411.07987](#)].
- [108] Z.-R. Huang, F.M. Bhutta, N. Farooq, M.A. Paracha and Y. Li, *Reinvestigating the semileptonic $B \rightarrow D^{(*)} \tau \bar{\nu}_\tau$ decays in the model independent scenarios and leptiquark models*, *Phys. Rev. D* **111** (2025) 115035 [[arXiv:2501.03734](#)].
- [109] Y. Li and C.-D. Lü, *Recent Anomalies in B Physics*, *Sci. Bull.* **63** (2018) 267 [[arXiv:1808.02990](#)].
- [110] S. Bifani, S. Descotes-Genon, A. Romero Vidal and M.-H. Schune, *Review of Lepton Universality tests in B decays*, *J. Phys. G* **46** (2019) 023001 [[arXiv:1809.06229](#)].
- [111] F.U. Bernlochner, Z. Ligeti, M. Papucci and D.J. Robinson, *Combined analysis of semileptonic B decays to D and D*: $R(D^{(*)})$, $|V_{cb}|$, and new physics*, *Phys. Rev. D* **95** (2017) 115008 [[arXiv:1703.05330](#)].
- [112] D. Bigi, P. Gambino and S. Schacht, *$R(D^*)$, $|V_{cb}|$, and the Heavy Quark Symmetry relations between form factors*, *JHEP* **11** (2017) 061 [[arXiv:1707.09509](#)].
- [113] BELLE collaboration, *Measurement of $\mathcal{R}(D)$ and $\mathcal{R}(D^*)$ with a semileptonic tagging method*, *Phys. Rev. Lett.* **124** (2020) 161803 [[arXiv:1910.05864](#)].
- [114] BELLE-II collaboration, *Test of lepton flavor universality with measurements of $R(D^+)$ and $R(D^{*+})$ using semileptonic B tagging at the Belle II experiment*, *Phys. Rev. D* **112** (2025) 032010 [[arXiv:2504.11220](#)].
- [115] PARTICLE DATA GROUP collaboration, *Review of particle physics*, *Phys. Rev. D* **110** (2024) 030001.